Tocris Cookson (Bristol, UK). All other chemicals were commercial products of reagent grade.

Animals. All the experiments were performed according to the Guideline for Animal Experiments of Kyoto University. Generation of an HDC-deficient mouse strain was described previously (12). The $HDC^{+/+}$ and $HDC^{-/-}$ mice, originally generated with a mixed genetic background of 129/Sv and CD1, were backcrossed to the Balb/c strain by 6–8 generations. Experiments were performed using 8- to 12-wk-old female $HDC^{+/+}$ and $HDC^{-/-}$ mice, 8-wk-old female Balb/c mice, 8-wk-old $WBB6F_1$-W/W^+ (W/W^+), and $-W/W^V$ (W/W^V) mice. All strains except the HDC-deficient mice were obtained from Japan SLC (Hamamatsu, Japan). The low-histamine diet (ver. 3), which contains ~1 nmol/g histamine, was purchased from Nihon Nosan Kogyo K. K. (Yokohama, Japan). The histamine-enriched diet was prepared by adding 80 μmol/g histamine to the low-histamine diet. In histamine-ingestion experiments, mice were freely fed with the low-histamine diet before experiments and then switched to the histamine-enriched diet for 7 days. Significant increases in plasma histamine levels were confirmed under these conditions (low-histamine diet, 0.04 ± 0.01 μM; histamine-enriched diet, 11.3 ± 1.25 μM in $HDC^{-/-}$ mice). For the purpose of collecting tissues and peritoneal cells, these mice were killed by cervical dislocation.

Determination of histamine content. Spleens were minced to obtain single-cell suspensions. Spleen cells were homogenized in 50 mM potassium phosphate, pH 6.8, containing 0.1% Triton X-100. The homogenates were centrifuged at 17,000 *g* for 30 min at 4°C, and the supernatant was used for the measurement of histamine content as previously described (23). The histamine formed was separated on a cation exchange column, WCX-1 (Shimadzu, Kyoto, Japan), by high-performance liquid chromatography (HPLC) and then measured by the *o*-phtalaldehyde method (19).

Immunofluorescence study. Spleens from Balb/c mice were collected and treated with Bouin's fixative (Muto Pure Chemicals, Tokyo, Japan) for 24 h at 4°C. Sections (8 μm in thickness) were cut on a Jung Frigocut 3000E cryostat. The sections were incubated with an antihistamine antibody (1:100) and an anti-CD14 antibody (1:100) for 1 day at 4°C. The sections were then stained with an Alexa 488-conjugated anti-rabbit IgG antibody (1:100) and a rhodamine-conjugated anti-rat IgG antibody (1:100). The fluorescent images were analyzed using a confocal microscope (MRC-1024, Bio-Rad Laboratories, Hercules, CA).

Preparation of peritoneal macrophages. Cells in the peritoneal cavity of Balb/c mice were harvested by lavage of the cavities with 3 ml of sterile phosphate-buffered saline (PBS). Lavage fluids were centrifuged at 200 *g* for 5 min at 4°C, and the pellet was washed in 2 ml of PBS. The peritoneal cells were cultured in RPMI-1640 medium containing 10% heat-inactivated fetal bovine serum, 100 U/ml penicillin, and 0.1 mg/ml streptomycin for 1 h at 37°C to allow adhesion. A viability of >98% of the cells was confirmed by the trypan blue exclusion test.

Cell culture. A mouse macrophage cell line, RAW264.7, was grown in RPMI-1640 medium supplemented with 10% heat-inactivated fetal calf serum, 100 U/ml penicillin, and 0.1 mg/ml streptomycin, in 5% CO_2 at 37°C in a fully humidified atmosphere. Exponentially growing cells were used in all experiments.

Measurement of [^{3}H]histamine uptake. Peritoneal macrophages obtained from Balb/c mice or RAW264.7 cells were incubated in modified Eagle's medium containing 10 mM HEPES-NaOH, pH 7.3, or Krebs-Ringer-HEPES (KRH) buffer (10 mM HEPES-NaOH, pH 7.3, containing 120 mM NaCl, 4.7 mM KCl, 2.2 mM $CaCl_2$, 1.2 mM KH_2PO_4, 1.2 mM $MgSO_4$, and 1.0 mM glucose) for 10 min at 37°C. In sodium-free conditions, NaCl in the KRH buffer was replaced with LiCl. The cells were then incubated with [^{3}H]histamine (2.33 μCi/ml) in the presence of cold histamine for the indicated periods at 37°C. The cells were rinsed twice in ice-cold PBS and lysed with PBS containing 1% Triton X-100. The radioactivities of the resultant soluble fractions were measured by a liquid scintillation counter. For the selective permeabilization of the plasma membranes, the cells were treated with 20 μg/ml digitonin for 10 min at 25°C instead of Triton X-100. Under these conditions, >95% of lactate dehydrogenase (a cytosolic enzyme) activity and no immunoreactive bands with an antiprotein disulfide isomerase (luminal protein of the endoplasmic reticulum) on immunoblot analyses was recovered in the leak-out fractions.

RESULTS

Accumulation of dietary histamine in spleen cells. We previously reported that a high level of histamine was accumulated in the spleens of HDC-deficient mice, which have a mixed genetic background (129/Sv × CD1), given a histamine-enriched diet for 7 days (11). High levels of accumulated histamine were reproduced in the spleens of both $HDC^{+/+}$ and $HDC^{-/-}$ mice, which were backcrossed to the Balb/c strain by six to eight generations, under the same dietary conditions (Table 1). The increase in histamine content in these mice was comparable to the parental Balb/c mice. Because W/W^V mice, which lack tissue mast cells (17), exhibited a similar level of increase in histamine content to the W/W^+ mice and Balb/c mice, it is likely that tissue mast cells are not involved in this histamine uptake.

To identify the cell type responsible for histamine accumulation in the spleen, an immunofluorescence study using an antihistamine antibody was performed. Histamine-immunoreactive cells were observed in the red pulp of the spleens of Balb/c, $HDC^{+/+}$, and $HDC^{-/-}$ mice given a histamine-enriched diet (data not shown). Double staining using an antihistamine antibody and an anti-CD14 antibody revealed that a portion of the $CD14^+$ cells in the spleens of Balb/c mice was immunoreactive to an antihistamine antibody (Fig. 1).

Table 1. *Effects of dietary histamine on histamine content in spleens of Balb/c, $HDC^{+/+}$, $HDC^{-/-}$, W/W^+, and W/W^V mice*

Strain	Normal Diet	Histamine-Enriched Diet
Balb/c	8.47 ± 0.871	99.9 ± 8.02*
$HDC^{+/+}$	5.45 ± 2.44	71.2 ± 6.40*
$HDC^{-/-}$	1.86 ± 0.97	49.2 ± 3.69*
W/W^+	1.89 ± 0.225	71.5 ± 3.20*
W/W^V	0.238 ± 0.00892	118 ± 16.5*

The values are presented as means ± SE (n = 5). Each mouse was given a normal diet or a histamine-enriched diet (80 μmol/g) for 7 days, and tissue histamine content in the spleens (nmol/g tissue) was measured as described in the MATERIALS AND METHODS. *$P < 0.01$ is regarded as significant by Student's t-test.

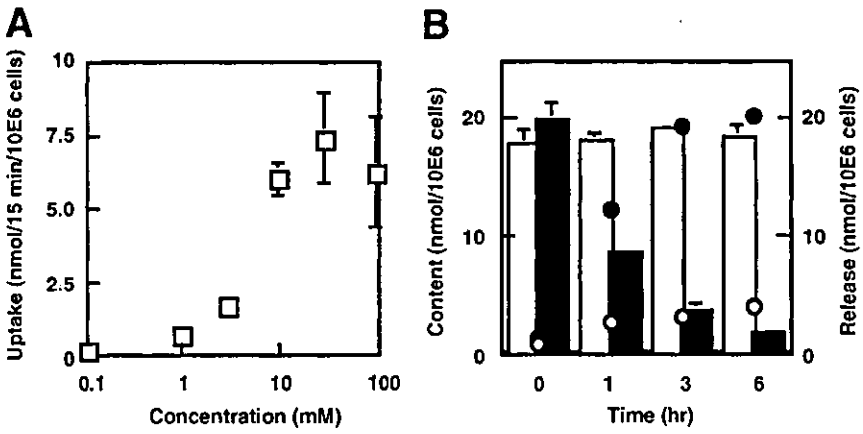

Fig. 3. Uptake and release of histamine by RAW264.7 cells. *A*: the concentration dependency of histamine uptake was investigated. RAW264.7 cells were incubated with [^{3}H]histamine (2.33 μCi/ml) in the presence of the indicated concentrations of cold histamine for 15 min. The values are presented as means ± SE (n = 3). *B*: RAW264.7 cells were incubated with 6 mM histamine for 2 h at 37°C. The cells were then washed twice and incubated in medium without histamine for the indicated periods at 37°C (filled columns, ●) or at 4°C (open columns, ○). Histamine in the cells (columns) and that in the medium (circles) were separated on a cation exchange column, WCX-1, and histamine content was evaluated by the *o*-phtalaldehyde fluorometric assay at each time point. The values are presented as means ± SE (n = 3).

Na^+-free conditions (Fig. 2*B*). The same experiments were performed using a mouse macrophage cell line, RAW264.7. The rate of histamine uptake in RAW264.7 cells was about 5 times higher than that in the peritoneal macrophages (Fig. 2*C*), and about 50% of this uptake was suppressed under Na^+-free conditions (Fig. 2*D*). Greater than 95% of the intracellular histamine was recovered in the soluble fraction of these cells and not in the membrane fraction (data not shown).

Dose-dependent accumulation of histamine in RAW264.7 cells. The dose-dependent accumulation of histamine in RAW264.7 cells was examined in the presence of various concentrations of histamine. Histamine uptake reached a plateau level at doses of >10 mM (Fig. 3*A*). The K_m value for histamine was calculated to be 6.0 mM in RAW264.7 cells and 5.6 mM in peritoneal macrophages (data not shown). RAW264.7 cells were found to accumulate a maximum of ~50 nmol of histamine/10^6 cells by 2 h of incubation at 37°C in the presence of 10 mM histamine, which is comparable to the levels of histamine stored in granules of mast cells (data not shown).

Release of histamine from RAW264.7 cells in the absence of extracellular histamine. To determine whether the accumulated histamine could be liberated from the cells, the cells were incubated in the presence of 6 mM histamine for 2 h, washed twice in histamine-free medium, and incubated for the indicated periods in the absence of extracellular histamine. Intracellular histamine leaked out into the medium within 6 h at 37°C, but not at 4°C (Fig. 3*B*). A good correlation was found between the decrease in histamine content in the cells and the increase in the medium. Furthermore, no metabolites of histamine were detected after 6 h of incubation on the basis of HPLC analyses (data not shown).

Distribution of accumulated histamine in RAW264.7 cells. We then investigated the subcellular distribution of accumulated histamine by an immunofluorescence study using the antihistamine antibody. Immunoreactive signals were observed in the cells incubated in the presence of histamine, but not in the absence of histamine (Fig. 4). The immunofluorescent signals observed with the antihistamine antibody largely colocalized with that observed with an antibody against Hsc70, which is a cytosolic molecular chaperone. Digitonin treatment, which is often used for selective permeabilization of plasma membranes, resulted in a rapid and complete release of accumulated histamine (1% Triton X-100; 100 ± 0.687%, 20 μg/ml Digitonin; 101 ± 8.38%). These results strongly indicate that histamine is accumulated in the cytosolic compartment of RAW2674.7 cells.

Effects of inhibitors of cytoskeletal activity on histamine uptake. Because macrophages are known to be active with regard to fluid-phase endocytosis, it is pos-

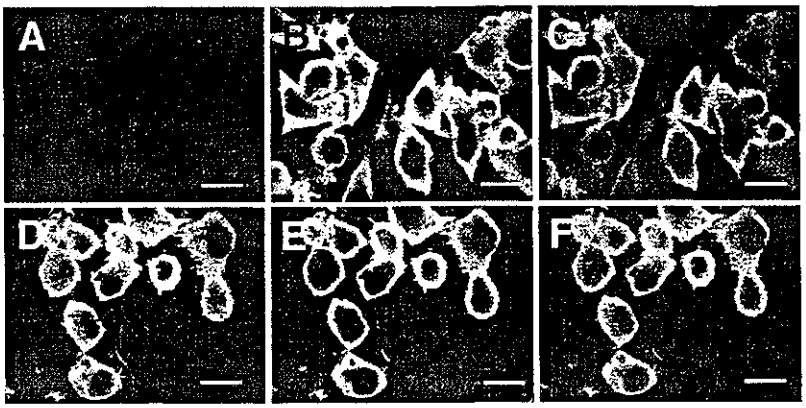

Fig. 4. Distribution of accumulated histamine in RAW264.7 cells. RAW264.7 cells were incubated for 2 h at 37°C in the presence (*D*, *E*, and *F*) or absence (*A*, *B*, and *C*) of 6 mM histamine. An immunofluorescence study was performed, using an antihistamine antibody (1:500; *A* and *D*) and an anti-heat shock cognate 70 antibody (1:1,000; *B* and *E*) as the primary antibodies, and stained by secondary antibodies (an Alexa 488-conjugated anti-rabbit IgG antibody, 1:200; *A* and *D*, an Alexa 546-conjugated anti-rat IgG antibody, 1:250; *B* and *E*). Fluorescent images were obtained using a confocal microscope (MRC-1024). A superimposed image is shown in *C* and *F*. Bars = 10 μm.

Table 2. *Effects of inhibitors of cytoskeletal activity on histamine uptake by RAW264.7 cells*

Inhibitors	Concentration, μg/ml	Histamine Uptake
None		100 ± 3.17
Colchicine	1	106 ± 3.52
	10	92.4 ± 6.56
Nocodazole	2	84.2 ± 7.42
Cytochalasin D	4	105 ± 7.52

The values are presented as means ± SE (n = 5). RAW264.7 cells were incubated for 15 min at 37°C with 6 mM histamine containing [^{3}H]histamine (2.33 μCi/ml) in the presence of the indicated concentrations of various inhibitors of cytoskeletal activity. The amounts of [^{3}H]histamine uptake are presented as a percentage of the control (None).

sible that this histamine uptake reflects a pinocytotic or endocytotic process. We performed uptake experiments using a series of inhibitors for cytoskeletal activity, such as colchicine, nocodazole, and cytochalasin D, to verify this hypothesis (Table 2). RAW264.7 cells were pretreated with each inhibitor for 30 min, and histamine uptake was measured in the presence of the inhibitor. No inhibitors were found to effectively block histamine uptake by RAW264.7 cells, excluding the possibility of the involvement of cytoskeletal reorganization and, hence, a pinocytotic or endocytotic process in histamine uptake.

Characterization of histamine uptake. To evaluate the substrate specificity in this histamine uptake by RAW264.7 cells, competitive analyses for histamine uptake in the presence of various concentrations of organic cations and compounds structurally related to histamine were performed. The histamine uptake into RAW264.7 cells at 6 mM was inhibited by both dopamine and serotonin (apparent K_i value, 25 mM and 20 mM, respectively). However, such inhibition was not observed in the case of histidine or GABA (Fig. 5*A*). Histamine uptake was markedly inhibited by pyrilamine or chlorpromazine (apparent K_i value, 0.60 and 0.20 mM), although terfenadine did not exhibit such inhibitory effects. An atypical antipsychotic drug, clozapine, which has recently been reported to be a weak agonist of the H_4 receptor (10), had no effects on histamine uptake at least up to 0.3 mM (Fig. 5*B*). The H_2 receptor ligand, dimaprit, famotidine, and cimetidine, did not exhibit inhibitory effects on histamine uptake at doses up to 3 mM. N^{α}-methylhistamine showed the same inhibitory potential as histamine, whereas thioperamide did not inhibit histamine uptake at doses of up to 1 mM (Fig. 5*C*). Although both tetraethylammonium (TEA) and 1-methyl-4-phenylpyridinium (MPP^+) have been reported to be good substrates for Na^+-independent organic cation transporters (7), these compounds did not inhibit histamine uptake in RAW264.7 cells (Fig. 5*D*). Quinidine significantly inhibited histamine uptake (apparent K_i value, 0.25 mM), whereas guanidine and L-carnitine did not. Chloroquine dose dependently suppressed histamine uptake. Histamine uptake was also suppressed (70.0 ± 4.51% of control) after intracellular acidification by preloading the cells for 15 min with 30 mM NH_4Cl, according to the procedure reported previously (2).

DISCUSSION

Various kinds of cells, such as mast cells, basophils, enterochromaffin-like cells, and histamine neurons, are known to produce and store histamine. We have found that a significant amount of histamine was accumulated in the spleens of various strains of mice, including the HDC-deficient mice, when they were maintained on a histamine-enriched diet for 7 days. Because the HDC-deficient mice showed no detectable de novo synthesis of histamine, and a very low enzymatic activity of HDC has been reported in the spleens

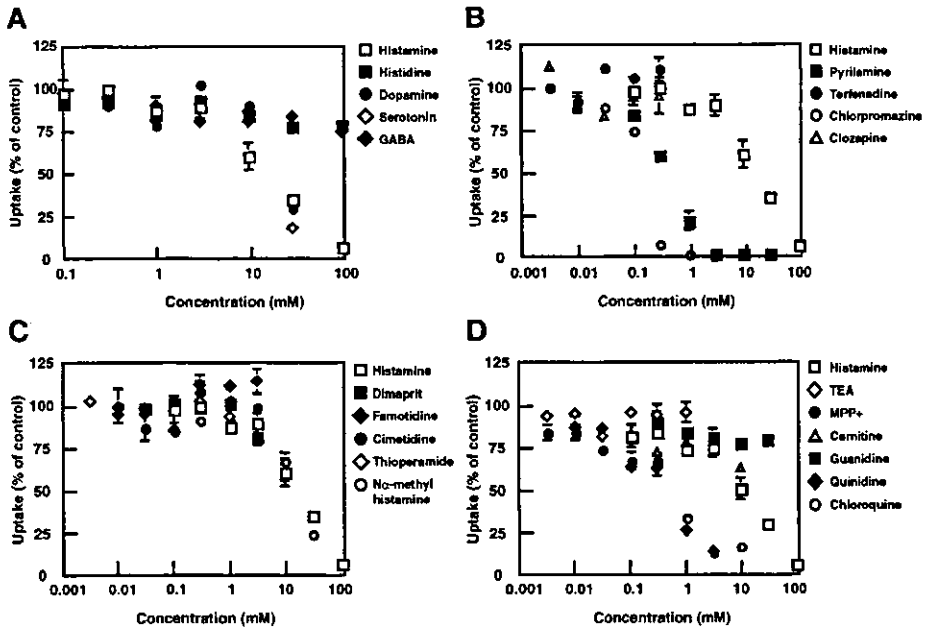

Fig. 5. Specificity of histamine uptake by RAW264.7 cells. RAW264.7 cells were incubated for 15 min at 37°C with 6 mM histamine containing [^{3}H]histamine (2.33 μCi/ml) in the presence of the indicated concentrations of a series of organic cations and compounds structurally related to histamine (*A–D*). The amounts of [^{3}H]histamine uptake are presented as percentages of the control. The profile of uptake in the presence of cold histamine is superimposed for comparison in each panel. Some compounds could not be tested in the full range of concentrations because of their low solubility or cytotoxicity at higher concentrations. The values are presented as means ± SE (n = 3). TEA, tetraethylammonium; MPP^+, 1-methyl-4-phenylpyridinium.

of wild-type mice, de novo synthesis of histamine is unlikely to be involved in the accumulation of dietary histamine in the spleens. The largest pool of histamine in peripheral tissues apart from the stomach is known to be mast cells. We previously reported that mouse bone marrow-derived cultured mast cells have the potential to take up histamine, and this uptake is also characterized by its low affinity for histamine (apparent K_m value, 1.6 mM) (11). However, because the increase in histamine accumulation was also observed in W/W^V mice, which lack tissue mast cells (17), mast cells are likely not to be involved in accumulation in the spleen. An immunohistochemical study using an antihistamine antibody indicated that a portion of the $CD14^+$ cells may be involved in histamine storage, although histamine uptake by mouse whole splenocytes was undetectable in our assay system (data not shown). This result indicates that only a small population of spleen cells may be able to take up histamine, although the subpopulations of $CD14^+$ cells in the spleen still remain largely unknown. Activated whole spleen cells with lipopolysaccharide were also found to be incapable of histamine uptake, as well as unstimulated spleen cells (data not shown).

Corbel et al. (4) demonstrated that mouse bone marrow cells were capable of histamine uptake and that splenocytes, thymocytes, and peritoneal cells were not. Regarding the histamine uptake by peritoneal cells, there seems to be a discrepancy between Corbel et al. and us, which may be a result of a difference in the cell populations used; Corbel et al. used whole peritoneal cells, whereas we separated peritoneal macrophages by their adhesion in this study. Mouse peritoneal macrophages and a macrophage cell line, RAW264.7, both of which are known to be $CD14^+$ cells, were found to be capable of histamine uptake. The uptake of histamine in peritoneal macrophages was found to be solely Na^+ independent, whereas that in RAW264.7 cells was significantly decreased in the absence of extracellular Na^+. However, the apparent K_m values for histamine were not different in the presence and in the absence of extracellular Na^+ (8.2 vs. 8.3 mM, data not shown). Although the rate of histamine uptake by peritoneal macrophages was lower than that by RAW264.7 cells, it was not influenced by the presence of extracellular Na^+. We performed further analyses using RAW264.7 cells to exclude the possibility that a small population of contaminating cells may interfere with the characterization of histamine uptake.

Recently, a family of nonneuronal organic cation transporters (OCT1, OCT2, OCT3, OCTN1, and OCTN2) has been cloned and characterized in mammalian expression systems (7). This family has been found to transport a variety of organic cations with high capacity in a Na^+-independent manner. Gründemann et al. (6) reported that histamine is a possible substrate of rat OCT2 and human EMT (OCT3). However, histamine uptake by RAW264.7 cells was not inhibited by MPP^+, although Gründemann et al. have demonstrated the competition between MPP^+ and histamine in a mammalian expression system. The expression of some OCT family members has been reported in limited tissues (5, 8, 14, 21, 22, 27), and there have been no reports about their expression in macrophages. Yabuuchi et al. (28) demonstrated that quinidine and pyrilamine are substrates for OCTN1. We detected by RT-PCR analyses very low levels of mRNA expression of OCTN1, abundant expression of OCTN2, and no expression of OCTN3 in RAW264.7 cells (data not shown), indicating that OCTN1 and OCTN2 are possible candidates for histamine uptake. However, histamine uptake by RAW264.7 cells was not inhibited by TEA, which is recognized as a substrate by all of the functionally active OCT family members, including OCTN1 and OCTN2 (5, 8, 14, 21, 22, 27). These results suggest that histamine uptake by RAW264.7 cells is mediated by a carrier distinct from the known OCT family members.

It is unlikely that histamine uptake by RAW264.7 cells is mediated by the internalization of histamine receptors, because no specific ligands to the histamine receptors could inhibit this uptake and little binding of histamine to the membrane fractions of the cells was observed. Two H_1 receptor ligands, pyrilamine and chlorpromazine, significantly inhibited histamine uptake, although another H_1 antagonist, terfenadine, did not. Furthermore, inhibition of histamine uptake by the other monoamines, dopamine, and serotonin indicates that this uptake system may function as an organic cation uptake system, which is not specific for histamine.

Because macrophages have been reported to possess active pinocytotic and endocytotic uptake systems, it is possible that histamine uptake may be dependent on these kinds of fluid-phase endocytosis. However, the inhibitors for cytoskeletal activity, such as colchicine, nocodazole, and cytochalasin D, which are known to suppress the pinocytotic and endocytotic process in macrophages (15, 20), were unable to block histamine uptake by RAW264.7 cells. This observation indicates that fluid-phase endocytosis may not be involved in the uptake of histamine.

Vestal et al. (24) reported the active uptake of propranolol by rabbit alveolar macrophages, which share some characteristics with histamine uptake in RAW264.7 cells: both are temperature dependent, inhibited by ammonium chloride and chloroquine, and effectively competed by chlorpromazine. Because Vestal et al. did not investigate the inhibitory effects of the endogenous amines, including histamine on propranolol uptake, it is unclear whether histamine uptake by RAW264.7 cells utilizes this system.

Histamine uptake by RAW264.7 cells was characterized by its low affinity and high capacity for histamine. Therefore, the physiological relevance of this uptake system may be limited to the clearance of a large amount of histamine release in the microenvironment, such as that through the degranulation of mast cells. Mast cells are often observed adjacent to macrophages in several tissues, such as the peritoneal cavity and lung, and it is possible that local concentrations of histamine reach millimolar levels around mast cells

upon activation. The role of histamine uptake by macrophages may be temporal elimination, because histamine accumulated in RAW264.7 cells was found to be intact and to be released into the medium in the absence of extracellular histamine. A drastic increase in the serum concentrations of histamine, which is usually observed in IgE-dependent systemic anaphylaxis, has been reported to result in altered respiratory frequency and hypothermia (9). The temporal storage of histamine in macrophages may function as a buffer system to prevent rapid and drastic changes in histamine concentrations during allergic responses, although further experimental evidence is required to elucidate the physiological roles of histamine uptake by macrophages.

In summary, we have found that dietary histamine is accumulated, especially in the spleen of mice. Immunohistochemical analyses suggest that a portion of the $CD14^+$ cells in the spleen may be involved in this histamine storage. Furthermore, mouse peritoneal macrophages and a mouse macrophage cell line, RAW264.7, have the potential to take up histamine, which may be one of the clearance systems of histamine.

We thank A. Popiel for help in preparation of the manuscript.

DISCLOSURES

This study was supported by grants-in-aid for Scientific Research from the Ministry of Education, Science, Sports, and Culture, Japan.

REFERENCES

1. **Beaven MA.** Histamine. *N Engl J Med* 294: 320–325, 1976.
2. **Brokl OH, Martinez CL, Shuprisha A, Abbott DE, and Dantzler WH.** Regulation of intracellular pH in proxymal tubules of avian long-looped mammalian-type nephrons. *Am J Physiol Regul Integr Comp Physiol* 274: R1526–R1535, 1998.
3. **Code CF.** Histamine and gastric acid secretion: a later look, 1955–1965. *Fed Proc* 24: 1311–1321, 1965.
4. **Corbel S, Schneider E, Lemoine FM, and Dy M.** Murine hematopoietic progenitors are capable of both histamine synthesis and uptake. *Blood* 86: 531–539, 1995.
5. **Gründemann D, Gorboulev V, Gambaryan S, Veyhl M, and Koepsell H.** Drug excretion mediated by a new prototype of polyspecific transporter. *Nature* 372: 549–552, 1994.
6. **Gründemann D, Liebich G, Kiefer N, Köster S, and Schömig E.** Selective substrates for non-neuronal monoamine transporters. *Mol Pharmacol* 56: 1–10, 1999.
7. **Inui K, Masuda S, and Saito H.** Cellular and molecular aspects of drug transport in the kidney. *Kidney Int* 58: 944–958, 2000.
8. **Kekuda R, Prasad PD, Wu X, Wang H, Fei YJ, Leibach FH, and Ganapathy V.** Cloning and functional characterization of a potential-sensitive polyspecific organic cation transporter (OCT3) most abundantly expressed in placenta. *J Biol Chem* 273: 15971–15979, 1998.
9. **Makabe-Kobayashi Y, Hori Y, Adachi T, Ishigaki-Suzuki S, Kikuchi Y, Kagaya Y, Shirato K, Nagy A, Ujike A, Takai T, Watanabe T, and Ohtsu H.** The control effect of histamine on body temperature and respiratory function in IgE-dependent systemic anaphylaxis. *J Allergy Clin Immunol* 110: 298–303, 2002.
10. **Oda T, Morikawa N, Saito Y, Masuho Y, and Matsumoto S.** Molecular cloning and characterization of a novel type of histamine receptor preferentially expressed in leukocytes. *J Biol Chem* 275: 36781–36786, 2000.
11. **Ohtsu H, Kuramasu A, Tanaka S, Terui T, Hirasawa N, Hara M, Makabe-Kobayashi Y, Yamada N, Yanai K, Sakurai E, Okada M, Ohuchi K, Ichikawa A, Nagy A, and Watanabe T.** Plasma extravasation induced by dietary supplemented histamine in histamine-free mice. *Eur J Immunol* 32: 1698–1708, 2002.
12. **Ohtsu H, Tanaka S, Terui T, Hori Y, Makabe-Kobayashi Y, Pejler G, Tchougounova E, Hellman L, Gertsenstein M, Hirasawa N, Sakurai E, Buzas E, Kovacs P, Csaba G, Kittel A, Okada M, Hara M, Mar L, Numayama-Tsuruta K, Ishigaki-Suzuki S, Ohuchi K, Ichikawa A, Falus A, Watanabe T, and Nagy A.** Mice lacking histidine decarboxylase exhibit abnormal mast cells. *FEBS Lett* 502: 53–56, 2001.
13. **Okinaga S, Ohrui T, Nakazawa H, Yamauchi K, Sakurai E, Watanabe T, Sekizawa K, and Sasaki H.** The role of HMT (histamine *N*-methyltransferase) in airways: a review. *Methods Find Exp Clin Pharmacol* 17: 16–20, 1995.
14. **Okuda M, Saito H, Urakami Y, Takano M, and Inui K.** cDNA cloning and functional expression of a novel rat kidney organic cation transporter, OCT2. *Biochem Biophys Res Commun* 224: 500–507, 1996.
15. **Pratten MK and Lloyd JB.** Pinocytosis and pahgocytosis: the effect of size of a particulate substrate on its mode of capture by rat peritoneal macrophages cultured in vitro. *Biochim Biophys Acta* 881: 307–313, 1986.
16. **Recsei PA and Snell EE.** Histidine decarboxylase of Lactobacillus 30a. *Virology* 9: 1492–1497, 1970.
17. **Reith AD and Bernstein A.** Molecular biology of the W and Steel loci. In: *Genome Analysis: Genes and Phenotypes*, edited by Davies KE and Tilghman SM. Cold Spring Harbor: Cold Spring Harbor Press, 1991, vol. 3, p. 105–131.
18. **Schwartz JC, Pollard H, and Quach TT.** Histamine as a neurotransmitter in mammalian brain: neurochemical evidence. *J Neurochem* 35: 26–33, 1980.
19. **Shore PA, Burkhalter A, and Cohn V.** A method for the fluorometric assay of histamine in tissues. *J Pharmacol Exp Ther* 127: 182–186, 1959.
20. **Swanson J, Burke E, and Silverstein SC.** Tubular lysosomes accompany stimulated pinocytosis in macrophages. *J Cell Biol* 104: 1217–1222, 1987.
21. **Tamai I, Ohashi R, Nezu J, Yabuuchi H, Oku A, Shimane M, Sai Y, and Tsuji A.** Molecular and functional identification of sodium ion-dependent, high affinity human carnitine transporter OCTN2. *J Biol Chem* 273: 20378–20382, 1998.
22. **Tamai I, Yabuuchi H, Nezu J, Sai Y, Oku A, Shimane M, and Tsuji A.** Cloning and characterization of a novel human pH-dependent organic cation transporter, OCTN1. *FEBS Lett* 419: 107–111, 1997.
23. **Tanaka S, Nemoto K, Yamamura E, and Ichikawa A.** Intracellular localization of the 74- and 53-kDa forms of L-histidine decarboxylase in a rat basophilic/mast cell line, RBL-2H3. *J Biol Chem* 273: 8177–8182, 1998.
24. **Vestal RE, Kornhauser DM, and Shand DG.** Active uptake of propranolol by isolated alveolar macrophages and its inhibition by other basic amines. *J Pharmacol Exp Ther* 214: 106–111, 1980.
25. **White MV.** The role of histamine in allergic diseases. *J Allergy Clin Immunol* 86: 599–605, 1990.
26. **Wolvekamp MC and de Bruin RW.** Diamine oxidase: an overview of historical, biochemical and functional aspects. *Dig Dis* 12: 2–14, 1994.
27. **Wu X, Prasad PD, Leibach FH, and Ganapathy V.** cDNA sequence, transport function, and genomic organization of human OCTN2, a new member of the organic cation transporter family. *Biochem Biophys Res Commun* 246: 589–595, 1998.
28. **Yabuuchi H, Tamai I, Nezu J, Sakamoto K, Oku A, Shimane M, Sai Y, and Tsuji A.** Novel membrane transporter OCTN1 mediates multispecific, bidirectional, and pH-dependent transport of organic cations. *J Pharmacol Exp Ther* 289: 768–773, 1999.

BIOLOGY OF REPRODUCTION 68, 804–811 (2003)
Published online before print 23 October 2002.
DOI 10.1095/biolreprod.102.003590

Expression of Messenger RNA for Prostaglandin E Receptor Subtypes EP4/EP2 and Cyclooxygenase Isozymes in Mouse Periovulatory Follicles and Oviducts During Superovulation[1]

Eri Segi, Kayo Haraguchi, Yukihiko Sugimoto, Masayuki Tsuji, Hiroko Tsunekawa, Shigero Tamba, Kazuhito Tsuboi, Satoshi Tanaka, and Atsushi Ichikawa[2]

Department of Physiological Chemistry, Graduate School of Pharmaceutical Sciences, Kyoto University, Sakyo-ku, Kyoto 606-8501, Japan

ABSTRACT

Prostaglandin (PG) E_2 is synthesized from arachidonic acid by cyclooxygenase (COX) and acts as a regulator in ovulation and fertilization reactions. We present the temporal and regional expression patterns of mRNAs for the two Gs-coupled PGE receptors, EP2 and EP4, and for COX-1 and COX-2 in mouse periovulatory follicles and oviducts during superovulation. Analysis using reverse transcription polymerase chain reaction revealed that the mouse ovaries express a significant amount of EP4 mRNA in addition to EP2 mRNA during superovulation. In situ hybridization results revealed that the signals for EP4 mRNA were localized mostly to oocytes in the preantral follicles. Three hours after hCG injection, the signals for EP4 and EP2 mRNA were present in both granulosa and cumulus cells. However, 9 h after hCG injection, just before ovulation, the signals for EP4 mRNA were still detectable in both cell types, whereas those for EP2 mRNA were found only in cumulus cells. COX-2 mRNA expression was present in both granulosa and cumulus cells at 3 h but was present only in cumulus cells at 9 h. COX-1 mRNA expression was not found in granulosa cells at 3 h but was found in these cells at 9 h. In the oviduct, the expression of EP4 and COX-1 mRNA was localized to epithelial cells, whereas expression of EP2 mRNA was localized to the smooth muscle layer. The tightly regulated expression of both EP2 and EP4 in the preovulatory follicles may reflect the essential role of PGE_2 in the ovulation process.

cumulus cells, granulosa cells, ovary, oviduct, ovulation

INTRODUCTION

Prostanoids are known as local mediators involved in various reproductive processes, such as ovulation, fertilization, implantation, and decidualization [1, 2]. These mediators are synthesized from arachidonic acid by the actions of cyclooxygenase (COX) and various prostaglandin (PG)-specific synthases. Nonsteroidal anti-inflammatory drugs (NSAIDs) such as aspirin and indomethacin inhibit ovulation in many species, including the mouse, rat, and rabbit [1, 3]. Of the two COX isozymes [4], COX-2 is induced in preovulatory follicles about 10 h prior to the start of follicular rupture, at least in the horse, cow, and rat [5–7]. These observations suggest that COX-2 acts as a molecular determinant of the time of ovulation [8]. Furthermore, analyses of the reproductive processes of COX-2-deficient (−/−) mice revealed a reduction in ovulation number and a severe failure in fertilization [9, 10]. Thus, COX-2-derived prostanoids are suspected to play pivotal roles in the physiological processes occurring during early pregnancy.

PGE_2, a dominant prostanoid in the ovary, reverses some of the inhibitory effects of NSAIDs or COX-2 gene deficiency. An LH surge leads to production of a large amount of PGE_2 within follicles [11]. These results indicate that some of the steps of ovulation are mediated by PGE_2. The actions of this prostanoid are mediated by PGE receptors comprising four subtypes: EP1, EP2, EP3, and EP4 [12]. These subtypes are encoded by different genes and differ in their signal transduction pathways; the EP1 subtype is coupled to Ca^{2+} mobilization, EP2 and EP4 to cAMP formation, and EP3 to inhibition of adenylate cyclase [13]. Although many investigators have indicated the importance of PGE_2 in the ovulation and fertilization processes, little is known about which receptor mediates the reproductive effects of PGE_2. We and other groups previously revealed that the EP2 receptor plays critical roles in these processes, especially in ovulation and fertilization, in EP2 −/− mice [14–17]. Furthermore, we found that EP2 mRNA is induced in cumulus cells by a gonadotropin surge and that EP2 −/− mice have a severe deficiency in cumulus expansion, which is required for successful fertilization. These findings and similar defects found in COX-2 −/− mice have clearly highlighted the importance of PGE_2 in ovulation and fertilization. However, no clear consensus has been established regarding localization and expression regulation of the PGE receptors in the ovarian follicles and oviducts during ovulation.

In this study, we focused on analysis of the temporal and regional expression patterns of mRNAs for EP4, EP2, and the COX isozymes in periovulatory follicles and oviduct of gonadotropin-treated mice during the ovulation period.

MATERIALS AND METHODS

Animals

All experiments were conducted in accordance with the ethical standards established by the institutional animal care and use committee Kyoto University. C57BL/6 mice were purchased from Japan SLC (Hamamatsu, Japan). Four-week-old female mice were housed under a 12L:12D cycle, with lights-on at 0800 h.

Superovulation

Five-week-old virgin mice, which were used as prepubertal animals, received a single i.p. injection of 5 IU eCG. After 48 h, mice were g

[1]This work was supported in part by grants from the Mochida Memorial Foundation for Medical and Pharmaceutical Research, the Sankyo Foundation of Life Science, the Takeda Science Foundation, and the Ministry of Education, Culture, Sports Science and Technology of Japan.
[2]Correspondence. FAX: 81 75 753 4557;
e-mail: aichikaw@pharm.kyoto-u.ac.jp

Received: 14 January 2002.
First decision: 6 February 2002.
Accepted: 14 September 2002.

ISSN: 0006-3363. http://www.biolreprod.org

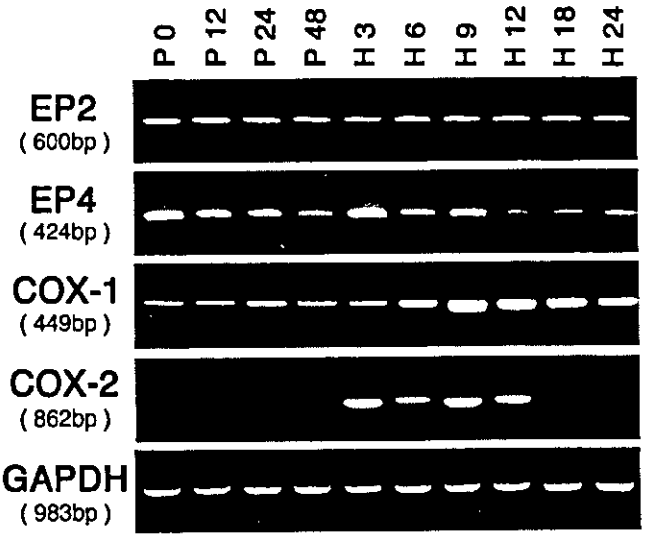

FIG. 1. Expression of mRNAs for the PGE receptors EP2 and EP4, and for COX isozymes in the mouse ovary during superovulation. One ovary was collected from each of four mice for each time point during superovulation. P0, P12, P24, and P48 indicate time (hours) after eCG injection; H3, H6, H9, H12, H18, and H24 indicate time (hours) after hCG injection. Ovaries were subjected to RT-PCR analysis; PCR products were electrophoresed on a 1.5% agarose gel and stained with ethidium bromide. The numbers of PCR cycles for ovarian RNA were 30, 28, 30, 30, and 25 for EP2, EP4, COX-1, COX-2, and GAPDH, respectively. All PCRs were confirmed to be in the logarithmic phase by monitoring the products obtained at the indicated number ± two cycles. The size of each band is indicated in parenthesis. Loading equivalence was verified by intensities of the GAPDH amplified products. RT-PCR analysis of ovaries isolated from eCG/hCG-treated mice was independently repeated three times from the preparation of ovaries, and similar results were obtained (data not shown).

an i.p. injection of 5 IU hCG. Mice were killed at different intervals after eCG or hCG treatment, and the ovaries and oviducts were isolated. Four ovaries from four mice were pooled for each time point and frozen in liquid nitrogen before RNA extraction. For in situ detection of mRNA expression, the ovary and oviduct were isolated and frozen in 2-isopentane at −50°C for preparation of sections and stored at −80°C until use. Cumulus-oocyte complexes (COCs) were isolated 48 h after eCG treatment or 3 and 9 h after hCG treatment by needling the ovaries in a 35-mm Petri dish containing saline with 0.3% BSA. Fourteen to 16 COCs were isolated from each of four animals for each time point. The COCs were pooled per animal, and RNA was extracted separately for each animal.

Reverse Transcription Polymerase Chain Reaction Analysis

Ovarian total RNA was isolated by the acid guanidinium thiocyanate-phenol-chloroform method [18], and total RNA from COCs was isolated by using the RNeasy Mini Kit (Qiagen Ltd., Valencia, CA). Complementary DNA was synthesized from ovarian total RNA (10 μg) and COC total RNA by using Moloney murine leukemia virus reverse transcriptase and the Superscript first-strand synthesis system (Invitrogen, Carlsbad, CA), respectively. Polymerase chain reaction (PCR) was performed using a GeneAmp PCR system 9700 (Perkin Elmer Applied Biosystems, Foster City, CA). Primers used in the PCR for EP1, EP2, EP3, EP4, COX-1, COX-2, and glyceraldehyde phosphate dehydrogenase (GAPDH) genes were as follows: EP1, 5′-ACC CTG CAT CCT GAG CAG CAC TGG CCC TCT-3′ (sense primer) and 5′-CGA TGG CCA ACA CCA CCA ACA CCA GCA GGG-3′ (antisense); EP2, 5′-TTC ATA TTC AAG AAA CCA GAC CCT GGT GGC-3′ (sense) and 5′-AGG GAA GAG GTT TCA TCC ATG TAG GCA TTG-3′ (antisense); EP3, 5′-ATC CTC GTG TAC CTG TCA CAG CGA CGC TGG-3′ (sense) and 5′-TGC TCA ACC GAC ATC TGA TTG AAG ATC ATT-3′ (antisense); EP4, 5′-GAC TGG ACC ACC AAC GTA ACG GCC TAC GCC-3′ (sense) and 5′-ATG TCC TCC GAC TCT CTG AGC AGT GCT GGG-3′ (antisense); COX-1, 5′-TGC ATG TGG CTG TGG ATG TCA TCAA-3′ (sense) and 5′-CAC TAA GAC AGA CCC GTC ATC TCC A-3′ (antisense); COX-2, 5′-GAG TGG GGT GAT GAG CAA CTA TTC C-3′ (sense) and 5′-CTG TAG GGT TAA TGT CAT CTA GTC T-3′ (antisense); GAPDH, 5′-TGA AGG TCG GTG TGA ACG GAT TTG GC-3′ (sense) and 5′-CAT GTA GGC CAT GAG GTC CAC CAC-3′ (antisense). The reaction conditions for the PCRs were as follows: for EP2, EP3, EP4, COX-1, and COX-2, denaturation at 94°C for 48 sec, annealing at 60°C for 42 sec, and extension at 72°C for 90 sec; for EP1, denaturation at 94°C for 48 sec, annealing at 68°C for 42 sec, and extension at 72°C for 90 sec; for GAPDH, denaturation at 94°C for 48 sec, annealing at 70°C for 48 sec, and extension at 72°C for 60 sec. The numbers of PCR cycles for ovarian RNA were 30, 28, 30, 30, and 25 for EP2, EP4, COX-1, COX-2, and GAPDH, respectively. The cycle numbers for PCR analysis of COC total RNA were 33, 31, 30, 25 and 24 for EP2, EP4, COX-1, COX-2, and GAPDH, respectively. All PCRs were confirmed to be in the logarithmic phase by monitoring the products obtained at the indicated number ±2 cycles. PCR products were electrophoresed on a 1.5% agarose gel and stained with ethidium bromide. The reverse transcription PCR (RT-PCR) experiments were independently repeated three times from the same total RNA material.

In Situ Hybridization

Ovarian and oviductal sections (10-μm thickness) were cut on a Jung Frigocut 3000E cryostat (Leica Instruments, Nussloch, Germany) and thaw-mounted onto poly-L-lysine-coated glass slides. The sections were fixed in 4% formalin in PBS for 10 min, rinsed in PBS, and acetylated with 0.25% acetic anhydride in 0.1 M triethanolamine-0.9% NaCl for 10 min at room temperature. After dehydration sequentially in 70%, 95%, and 100% ethanol, the sections were air dried and stored at −80°C until use. Mouse cDNAs for EP2, EP4, COX-1, and COX-2 were subcloned into pBluescript II (Stratagene, La Jolla, CA) for synthesis of antisense and sense complementary RNA probes [19, 20]. Riboprobes were synthesized by transcription with T3 or T7 RNA polymerase (Stratagene) in the presence of [α-^{35}S]CTP. Cold antisense riboprobes were also synthesized by the same procedure using unlabeled nucleotides. Hybridization was carried out as described previously [19]. The specificity of the signal with each antisense probe was verified both by its disappearance with the addition of an excess of unlabeled probe and by the absence of specific hybridization with the sense probe (data not shown). Hybridization sec-

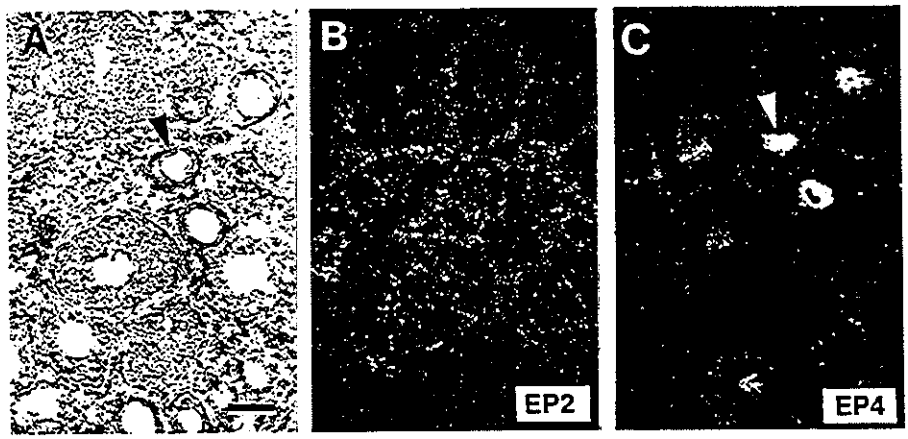

FIG. 2. Regional distribution of the mRNAs for the PGE receptors EP2 and EP4 in ovaries from prepubertal mice (before eCG treatment; P0 in Fig. 1) detected by in situ hybridization. A) Bright-field view of an immature ovary section (10 μm) stained with hematoxylin and eosin. B and C) Dark-field view of immature ovary sections hybridized with a ^{35}S-labeled antisense riboprobe for the EP2 (B) and EP4 (C) mRNA. These sections are adjacent to those in A. The white arrowhead pointing to EP4-hybridizing signals indicates an oocyte corresponding to the black arrowhead in A. Bar = 150 μm.

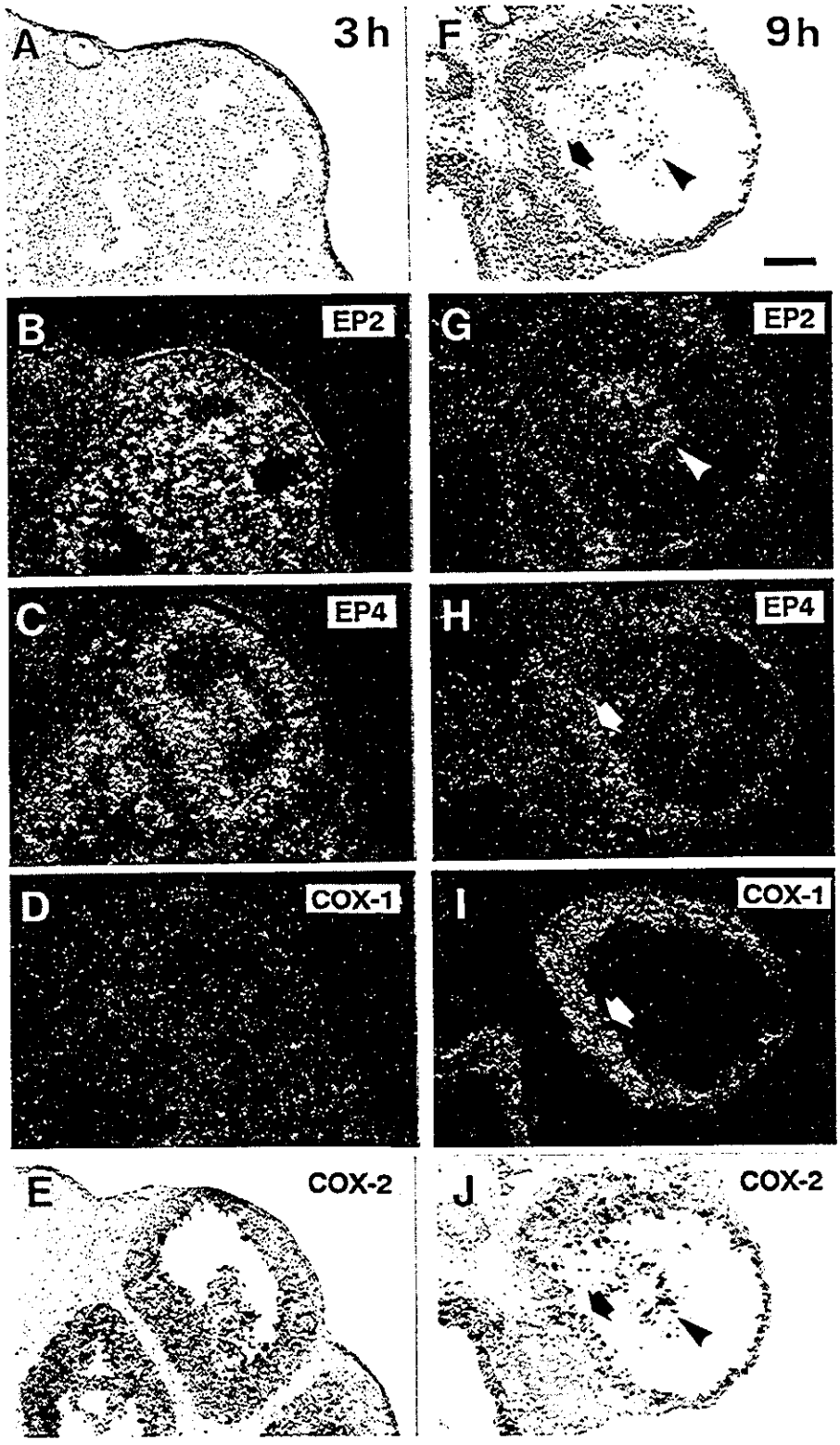

FIG. 3. Regional distribution and changes in the expression patterns of mRNAs for EP2, EP4, COX-1, and COX-2 in preovulatory follicles. In situ hybridization signals for PGE receptors and COX isozymes are shown in ovaries isolated from mice 3 h or 9 h after hCG administration (H3 and H9). The photomicrographs show the histology of preovulatory follicle sections stained with hematoxylin and eosin (**A** and **F**) and signals for EP2 mRNA (**B** and **G**), EP4 mRNA (**C** and **H**), COX-1 mRNA (**D** and **I**), and COX-2 mRNA (**E** and **J**). Hybridization signals are presented in the dark-field view (**B–D**, **G–I**), and in the bright-field view (**E** and **J**). These photomicrographs are from sequential sections at each time point. Arrowheads indicate the cumulus cells, and arrows indicate the granulosa cells (**F–J**). Bar = 150 μm.

tions were dipped in nuclear track emulsion (NTB3; Eastern Kodak Co., Rochester, NY). After exposure for 5 wk at 4°C, the dipped slides for all probes were developed, fixed, and counterstained with hematoxylin and eosin. Six sections were examined for the expression of each mRNA at each time point in each ovary and oviduct, and four ovaries and oviducts were examined per time. The in situ hybridization experiments were repeated independently three times, and similar results were obtained (data not shown). All data used in the figures and for quantification were from experiments with the same labeled probes.

Quantification of In Situ Signals and Statistical Analysis

The ratio of hybridization signal-positive area:total cell area (positive area ratio) was quantified using the Image-Pro Plus software (Me-

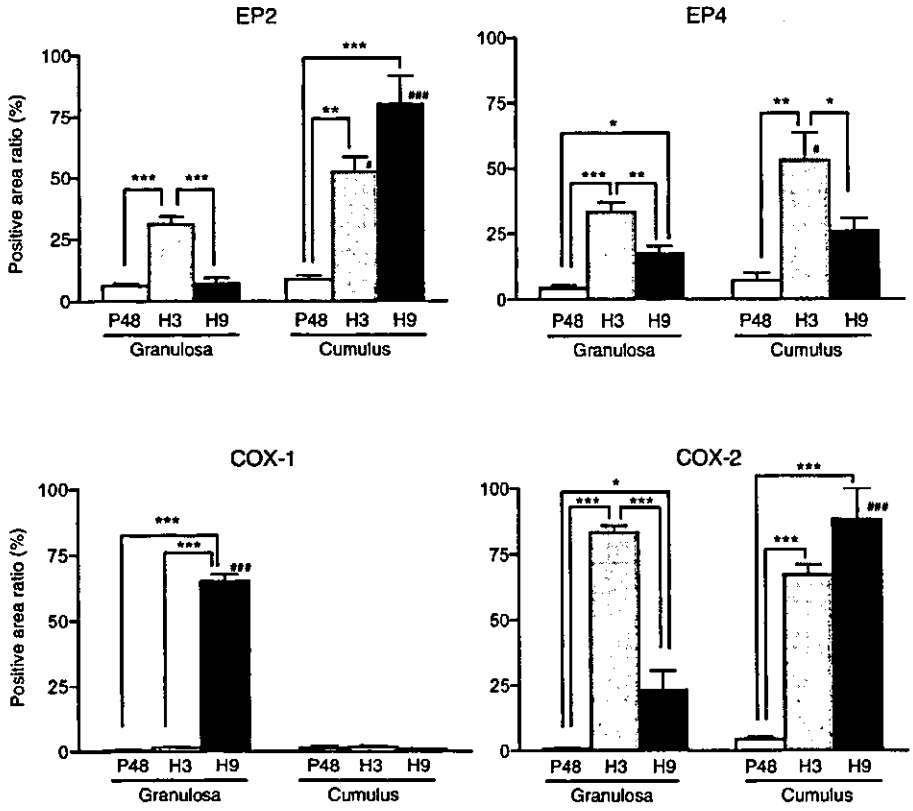

FIG. 4. Quantitative analysis of in situ hybridization results for expression of mRNA for EP2, EP4, COX-1, and COX-2 in mouse follicles at P48, H3, and H9. The positive area ratio was calculated as the percentage of number of pixels of signal area occupied by the silver grains per pixels of cell area within a marked area. Six to eight follicles from each of four ovaries were examined at each time point. All data are reported as the mean ± SEM and were analyzed using a two-way ANOVA (time and cell type) and the Bonferroni multiple comparison method as post hoc tests (*$P < 0.05$, **$P < 0.01$, ***$P < 0.001$ among hCG treatment times within the same cell type; #$P < 0.05$, ###$P < 0.001$ for granulosa cells vs. cumulus cells at the same treatment time).

dia Cybernetics, Silver Spring, MD). Within a marked area, the image analysis system determined the number of graphic pixels occupied by the silver grains (signal area) in the dark-field view. The program also counted the number of pixels occupied by the hematoxylin and eosin-stained area (cell area) within the marked area. Positive area ratio was then defined as the number of pixels of signal area per pixels of cell area. Six to eight follicles from each of four ovaries were examined at each time point. All data were reported as the mean ± SEM and were analyzed with a two-way ANOVA (time and cell type) and the Bonferroni multiple comparison method as post hoc tests. A P value of <0.05 was considered significant.

RESULTS

RT-PCR Analysis of the Expression of mRNAs for PGE Receptors EP1, EP2, EP3, and EP4 and for COX Isozymes in Mouse Ovaries

Using RT-PCR analysis, we first investigated the expression of mRNAs for the PGE receptors EP1, EP2, EP3, and EP4 and for the COX isozymes in the ovaries of prepubertal mice treated with eCG and hCG. EP2 mRNA was consistently detected in the ovaries of mice treated or not treated with gonadotropins (Fig. 1). However, EP4 mRNA was detected in nontreated immature ovaries (P0), and the amount gradually decreased after eCG treatment. At 3 h after hCG treatment (H3) the EP4 mRNA level was temporarily increased but was decreased again at 6 h (H6) and then increased again at 9 h (H9). For COX-2 mRNA, a rapid increase was observed at H3 in the mouse ovaries. This high expression level was decreased at H6 and then increased again at H9. Although COX-1 mRNA was expressed during all the time points examined, increased expression was obtained in ovaries from H9 to H18. Neither EP1 nor EP3 mRNA expression was detectable in ovaries from any time points (data not shown).

Because the expression levels of mRNAs for EP2, EP4,

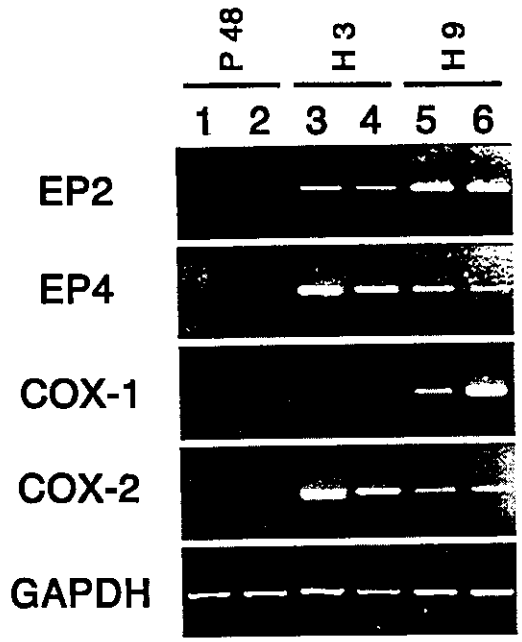

FIG. 5. Expression of mRNAs for EP2, EP4, COX-1, and COX-2 in COCs isolated 48 h after eCG treatment or 3 and 9 h after hCG treatment by needling the ovaries in a 35-mm Petri dish containing saline with 0.3% BSA. Fourteen to 16 COCs were isolated from each of four animals for each time point. The COCs were pooled per animal, and RNA was extracted separately for each animal. PCR conditions were the same as those in . The cycle numbers for PCR analysis were 33, 31, 30, 25, and 24 for EP2, EP4, COX-1, COX-2, and GAPDH, respectively. All PCRs were confirmed to be in the logarithmic phase by monitoring the products obtained at the indicated number ± two cycles. The numbers on the top (1–6) represent COC total RNA isolated from different animals. Six animals per time point were analyzed, and similar results were obtained.

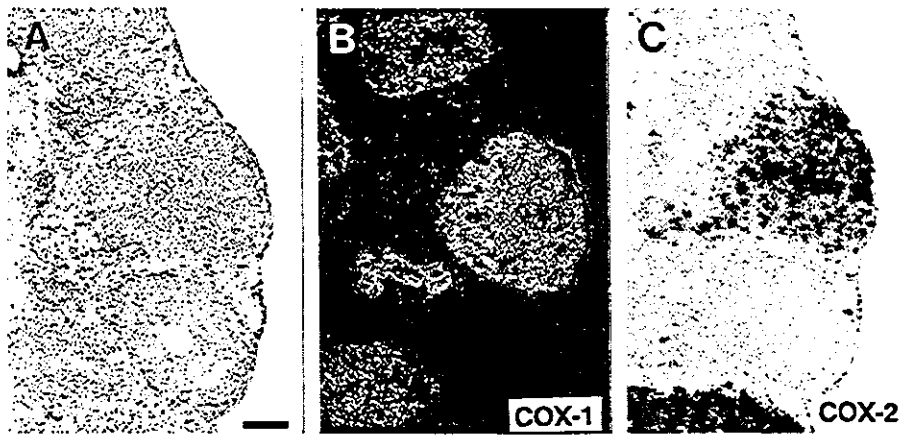

FIG. 6. Expression of mRNAs for COX-1 and COX-2 in granulosa cells after ovulation. Ovaries were isolated 12 h after hCG administration and subjected to in situ hybridization. The photomicrographs are sequential sections and show the histology of follicles just after ovulation stained with hematoxylin and eosin (A) and signals for COX-1 mRNA (B) and COX-2 mRNA (C). Hybridization signals are presented in the dark-field view (B, white grains) and in the bright-field view (C, black grains). Bar = 150 μm.

and the COX isozymes varied in a time-dependent manner in mouse ovaries after hCG treatment, the regional and cellular distribution of these mRNAs were determined by in situ hybridization analysis.

Cellular Localization of EP2, EP4, COX-1, and COX-2 mRNAs in Immature Ovaries

To investigate the cellular distribution of signals for EP2, EP4, COX-1, and COX-2 mRNA in immature ovarian tissue, in situ hybridization analysis was performed with immature ovaries from mice before injection of eCG. The signals for EP4 mRNA were localized mainly in oocytes of small preantral follicles (Fig. 2C), whereas the signals for EP2 mRNA were in the theca and interstitial area (Fig. 2B). Although faint signals for COX-1 mRNA appeared to be present in the interstitial cells, the cell population could not be identified because of the existence of a variety of cell types (data not shown). No significant signals for COX-2 mRNA were observed in the immature ovaries of mice (data not shown).

Cellular Localization of EP2, EP4, COX-1, and COX-2 mRNAs in Preovulatory Follicles

Human chorionic gonadotropin causes a variety of responses, such as cumulus expansion in the COCs and proteolysis in the follicular wall, that are required for successful ovulation. Histological sections of the mouse ovary were processed for in situ detection of mRNAs for EP2, EP4, COX-1, and COX-2 at the following time points: 48 h after eCG injection (P48); 3 h after hCG injection (H3), the period corresponding to significant induction of COX-2 mRNA by gonadotropin (Fig. 1); and 9 h after hCG injection (H9), the period corresponding to just before the time of ovulation. In the ovary at P48, the signals for EP4, COX-1, and COX-2 mRNAs were undetectable, and only faint signals for EP2 mRNA were observed in the theca and interstitial area as observed in immature ovaries (data not shown). In contrast, at H3 the signals for EP2 and EP4 mRNAs were detected mainly in both granulosa and cumulus cells (Fig. 3, B and C). In addition, faint but consistent signals for EP2 mRNA were still observed in theca cells and interstitial cells. In contrast to strong signals for COX-2 mRNA, COX-1 mRNA signals were not detected in these cell types (Fig. 3, D and E). In the H9 ovaries, the signals for EP2 mRNA were mainly localized to cumulus cells (Fig. 3G), and the signals for EP4 mRNA were localized to granulosa cells (Fig. 3H). At this time point, signals for COX-1 mRNA were seen in granulosa cells (Fig. 3I). Strong signals for COX-2 mRNA were detected at both H3 and H9 in the granulosa and cumulus cells (Fig. 3, E and J).

To quantitatively analyze the signals for EP2, EP4, COX-1, and COX-2 mRNAs in granulosa cells and cumulus cells at H3 and H9, the values of the positive area ratios were analyzed according to the procedures described in *Materials and Methods.* Each value of the positive area ratio for H3 or H9 was compared with that of P48 (Fig. 4). In H3 ovaries, the values for EP2, EP4, and COX-2 mRNAs were significantly elevated compared with values at P48 in both granulosa cells and cumulus cells. In the H9 ovaries compared with the H3 ovaries, the values for EP2 and COX-2 mRNAs were notably decreased in the granulosa cells but were maintained at high levels in cumulus cells. At this time, the values for EP2 and COX-2 mRNAs in cumulus cells were significantly higher than those in granulosa cells. In the H9 ovaries, the values for EP4 mRNA in both cell types were slightly decreased compared with those of H3 ovaries. In contrast, the value for COX-1 mRNA was significantly increased in the granulosa cells of H9 ovaries.

In situ hybridization revealed that the intensities of the signals for EP2 and EP4 mRNAs in H3 follicles were stronger than those in H9 follicles (Fig. 3, B vs. G, C vs. H), although the intensities of the PCR bands were not so different from each other (Fig. 1). To assess this inconsistency, we performed RT-PCR analysis using COCs corresponding to P48, H3, and H9 as starting material. None of the mRNAs for EP2, EP4, COX-1, or COX-2 could be detected at P48 under these PCR conditions (Fig. 5). With hCG treatment, the levels of both EP4 mRNA and EP2 mRNA expression were clearly increased in COCs in the H3 follicles. Thereafter, the expression of EP2 mRNA was further stimulated and that of the EP4 mRNA was diminished in COCs in H9 follicles. However, COX-2 signals were rapidly increased by hCG treatment in H3 follicles, and COX-1 signals gradually increased as seen in H9 follicles.

Cellular Localization of COX-1 and COX-2 mRNAs in Granulosa Cells of Follicles Just after Ovulation

At H9, in situ hybridization analysis revealed that the mRNA signals for the COX isozymes were expressed in granulosa cells of preovulatory follicles (Fig. 3, I and J). In the granulosa cells of H9 follicles, EP4 mRNA signals were apparent but those of EP2 mRNA were faint (Fig. 3, G and H). At 12 h after hCG injection, granulosa cells in the follicles start to differentiate into luteal cells. Therefore, expression of mRNAs for the COX isozymes and EP4 was

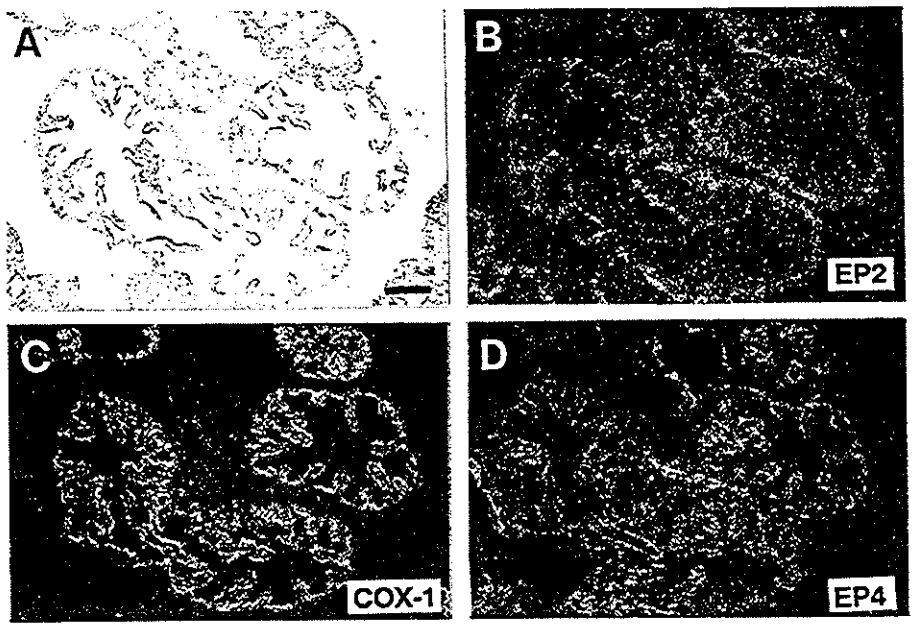

FIG. 7. Expression of EP2 mRNA in the oviductal muscle layer and expression of EP4 and COX-1 mRNA in the epithelium of the oviduct. Ovaries were isolated from mice 12 h after hCG administration and subjected to in situ hybridization. A) Bright-field view of a section stained with hematoxylin and eosin. B–D) Dark-field views showing signals for EP2 (B), COX-1 (C), and EP4 (D) mRNA. Bar = 150 μm.

examined in these cells. Messenger RNAs for COX-1 and COX-2 were still expressed in the granulosa cells of the ovulated follicles, as indicated by in situ hybridization analysis (Fig. 6). However, EP4 mRNA signals were not observed in these cells (data not shown).

Cellular Localization of EP2, EP4, and COX-1 mRNAs in the Oviduct

The oviduct is a tube extending from the periovarial space to the uterine horns. Ovulated COCs enter the oviduct and stay in the ampulla, where the fertilization processes occur. Cumulus cells in follicles strongly express both EP2 and COX-2 mRNA (Fig. 3, B and E). Such expression of EP2 and COX-2 mRNA in cumulus cells was still found in the ovulated COCs within the ampulla of the oviduct (data not shown). In the oviducts, the signals for EP2 mRNA were mainly localized to the smooth muscle layer (Fig. 7B), especially to the highly ciliated area of the tract near the ovary. The signals for EP4 mRNA were observed in the epithelium throughout the oviduct (Fig. 7D). The distribution of the signals for COX-1 mRNA corresponded roughly to that for EP4 mRNA (Fig. 7C). No significant signals for COX-2 mRNA were observed throughout the oviduct (data not shown).

DISCUSSION

Expression of mRNAs for the PGE Receptors EP4 and EP2 and for COX Isozymes in Preovulatory Follicles

The expression of the two COX isozymes and the two Gs-coupled EP receptors increased in particular follicle cells in response to gonadotropins. Expression of COX-2, EP2, and EP4 rapidly increased in both cumulus and granulosa cells 3 h after hCG injection, but cumulus cells dominantly expressed COX-2 and EP2 9 h after hCG treatment. COX-1 mRNA expression in granulosa cells was apparent only at 9 h after hCG administration. There is no doubt that the LH surge is a primary event leading to the induction of EP receptors and COX isozymes in preovulatory follicles, but the expression pattern is different for each between 3 h and 9 h. Because gonadotropins are known to stimulate the synthesis of various kinds of intrafollicular mediators [21], late induction or changes in expression may be mediated by other factors including PGs. In several cell types, COX-2-derived PGs stimulate COX-2 expression itself in an autocrine manner [22]. This positive feedback regulation by PGs may be a mechanism underlying distinct expression patterns between 3 h and 9 h.

Expression of EP4 and EP2 increased in both cumulus and granulosa cells as a gonadotropin-elicited rapid response (3 h). Although EP2-deficient mice but not EP4-deficient mice show a significant defect in the ovulation process [23], simultaneous induction of the two Gs-coupled PGE receptors suggested pivotal roles for PGE_2 in the ovulation process; EP2 and EP4 might cooperatively work as a compensatory system for successful ovulation. Follicular rupture involves a complex series of biochemical and biophysical changes in the theca cells, cumulus cells, and granulosa cells, which interact with each other [21]. Gonadotropin-elicited interstitial collagenase (matrix metalloprotease 1) induction in granulosa cells, which is regarded as a key step in follicular rupture, was suppressed by treatment with indomethacin [21, 24, 25]. Miyaura et al. [26] recently demonstrated that EP4 is responsible for the PGE_2-induced activation of matrix metalloproteases in mouse calvarian cells. EP2 and EP4 expressed in granulosa cells may play roles in ovulation in a similar fashion. Further analyses using EP-specific antagonists or EP2/EP4 double knockout mice are needed to evaluate the exact roles of PGE_2 through each receptor subtype.

The present study also highlights COX-1 expression in granulosa cells as a late response (9 h after ovulation). Although the induction of COX-2 gene expression has been identifed in the ovaries of various animals around the ovulation period [5–8, 27, 28], very few researchers have analyzed COX-1 expression during ovulation except for one study of whole rat ovaries [29]. The function of COX-1 mRNA expression just before ovulation is currently unknown. RT-PCR analysis (Fig. 1) indicated that COX-2 mRNA expression also showed an early (3 h) and a late (9 h) increase after hCG injection, which coincides with the observations previously reported by Joyce et al. [28]. These results suggest that granulosa cells start to express both

COX isozymes just before ovulation. Moreover, expression of COX-1 and COX-2 was detected in granulosa cells (corresponding to the cells differentiating into luteal cells) in follicles after ovulation (Fig. 6). Prostanoids synthesized by each enzyme may participate cooperatively in the final steps of the ovulation and/or postovulation processes.

We quantified the results in in situ hybridization by evaluating hybridization signal-positive area per total cell area to determine what percentage of the total cumulus or granulosa cells express a particular mRNA. This quantification analysis revealed that the value of the EP2-positive cells per total cumulus cells was higher in H9 ovaries than in H3 ovaries (see Fig. 4, *Cumulus* in panel EP2), even though the signal density for EP2 mRNA in the cumulus cells looked higher at H3 than at H9 (Fig. 3, B and G). The cumulus cells in H9 ovaries are less dense than those in H3 ovaries because of the cumulus expansion. Therefore, the sparse signals for EP2 mRNA in the cumulus cells of H9 ovaries reflect the lower cell density on this section apart from the ratio of EP2-positive cells to negative cells.

Expression of mRNAs for EP4 and EP2 in the Oviduct

Pharmacological experiments have demonstrated that exogenous PGE_2 is able to inhibit contractions of the oviductal tube in the rabbit [30] and to decrease passage pressure in the rat oviduct [31]. In the present study, we clearly demonstrated that EP2 mRNA is expressed in the muscle layer. These results suggest that PGE_2, via EP2, may contribute to relaxation of the oviduct, which is favorable for successful fertilization [32]. A severe defect in fertilization in EP2-deficient female mice may be partly due to a lack of effect of PGE_2 in the oviduct. However, oviductal epithelia secrete glycoproteins and produce a flow in oviductal fluid by ciliary action [33]. In the rabbit oviduct, PGE_2 stimulates ciliary activity in the epithelium [34]. PGE_2 also stimulates mucin exocytosis from intestinal epithelial cells via EP4 [35]. Thus, EP4 may regulate both the secretion of glycoproteins and ciliary activity in the oviductal epithelium. Such mechanisms may act favorably in the process of fertilization.

Expression of EP4 and EP2 mRNAs in Preantral Follicles

EP4 mRNA expression was found in oocytes within preantral follicles. Because transcripts in oocytes are sometimes translationally dormant and are activated in a time-dependent manner [36], it is not clear whether the EP4 receptor proteins are expressed in the oocytes at this stage. There is little information on the effects of prostanoids on oocyte function, and the role of EP4 in oocytes remains to be clarified. However, we detected faint but significant signals for COX-1 mRNA in the interstitial area (Fig. 1). Therefore, very low levels of PGE_2 may be constitutively synthesized by COX-1 and may act on EP4 in the oocytes at this stage.

EP4 mRNA is present in the cumulus and granulosa cells in the preovulatory follicles. COX-1 mRNA is expressed in the granulosa cells just before ovulation, in contrast to the preferred expression of EP2 and COX-2 mRNA in the cumulus cells. These results extend our knowledge of the expression of COX enzymes and PGE receptors and the possible active sites of PGE_2 in the female reproductive processes.

ACKNOWLEDGMENTS

We thank Drs. S. Yamamoto and K. Yamamoto (Tokushima University of Medical Science) for the gift of COX-1 and COX-2 cDNA.

REFERENCES

1. Murdoch WJ, Hansen TR, McPherson LA. A review—role of eicosanoids in vertebrate ovulation. Prostaglandins 1993; 46:85–115.
2. Viggiano JM, Herrero MB, Cebral E, Boquet MG, de Gimeno MF. Prostaglandin synthesis by cumulus-oocyte complexes: effects on in vitro fertilization in mice. Prostaglandins Leukotrienes Essent Fatty Acids 1995; 53:261–265.
3. Downs SM, Longo FJ. Effects of indomethacin on preovulatory follicle in immature, superovulated mice. Am J Anat 1982; 164:265–274.
4. Langenbach R, Loftin C, Lee C, Tiano H. Cyclooxygenase knockout mice. Models for elucidating isoform-specific functions. Biochem Pharmacol 1999; 58:1237–1246.
5. Sirois J, Simmons DL, Richards JS. Hormonal regulation of messenger ribonucleic acid encoding a novel isoform of prostaglandin endoperoxide H synthase in rat preovulatory follicles. J Biol Chem 1992; 267:11586–11592.
6. Boerboom D, Sirois J. Molecular characterization of equine prostaglandin G/H synthase-2 and regulation of its messenger ribonucleic acid in preovulatory follicles. Endocrinology 1998; 139:1662–1670.
7. Liu J, Carriere PD, Dore A, Sirois J. Prostaglandin G/H synthase-2 is expressed in bovine preovulatory follicles after the endogenous surge of luteinizing hormone. Biol Reprod 1997; 57:1524–1531.
8. Sirois J, Dore M. The rate of induction of prostaglandin G/H synthase-2 in equine preovulatory follicles supports its role as a determinant of the ovulatory process. Endocrinology 1997; 138:4427–4434.
9. Lim H, Paria BC, Das SK, Dinchuk JE, Langenbach R, Trzaskos JM, Dey SK. Multiple female reproductive failures in cyclooxygenase 2-deficient mice. Cell 1997; 91:197–208.
10. Davis BJ, Lennard DE, Lee CA, Tiano HF, Morhan SG, Wetsel WC, Langenbach R. Anovulation in cyclooxygenase-2-deficient mice is restored by prostaglandin E_2 and interleukin-1β. Endocrinology 1999; 140:2685–2695.
11. Mikuni M, Pall M, Peterson CM, Hellberg M, Brannstorm M, Richards JS, Hedin L. The selective prostaglandin endoperoxide synthase-2 inhibitor, NS-398, reduces prostaglandin production and ovulation in vivo and in vitro in the rat. Biol Reprod 1998; 59:1077–1083.
12. Coleman RA, Smith WL, Narumiya S. International Union of Pharmacology classification of prostanoid receptors: properties, distribution, and structure of the receptors and their subtypes. Pharmacol Rev 1994; 46:205–229.
13. Sugimoto Y, Narumiya S, Ichikawa A. Distribution and function of prostanoid receptors: studies from knockout mice. Prog Lipid Res 2000; 39:289–314.
14. Hizaki H, Segi E, Sugimoto Y, Hirose M, Saji T, Ushikubi F, Matsuoka T, Noda Y, Tanaka T, Yoshida N, Narumiya S, Ichikawa A. Abortive expansion of the cumulus and impaired fertility in mice lacking the prostaglandin E receptor subtype EP2. Proc Natl Acad Sci U S A 1999; 96:10501–10506.
15. Kennedy CRJ, Zhang Y, Brandon S, Guan Y, Coffee K, Funk CD, Magnuson MA, Oates JA, Breyer MD, Breyer RM. Salt-sensitive hypertension and reduced fertility in mice lacking the prostaglandin EP2 receptor. Nat Med 1999; 5:217–220.
16. Tilly SL, Audoly LP, Hicks FH, Kim HS, Flannery PJ, Coffman TM, Koller BH. Reproductive failure and reduced blood pressure in mice lacking the EP2 prostaglandin E_2 receptor. J Clin Invest 1999; 103:1539–1545.
17. Matsumoto H, Ma WG, Smalley W, Trzaskos J, Breyer RM, Dey SK. Diversification of cyclooxygenase-2-derived prostaglandins in ovulation and implantation. Biol Reprod 2001; 64:1557–1565.
18. Chomczynski P, Sacchi N. Single-step method of RNA isolation by acid guanidinium thiocyanate-phenol-chloroform extraction. Anal Biochem 1987; 162:156–159.
19. Katsuyama M, Sugimoto Y, Morimoto K, Hasumoto K, Fukumoto M, Negishi M, Ichikawa A. Distinct cellular localization of the messenger ribonucleic acid for prostaglandin E receptor subtypes in the mouse uterus during pseudopregnancy. Endocrinology 1997; 138:344–350.
20. Tsuboi K, Sugimoto Y, Iwane A, Yamamoto K, Yamamoto S, Ichikawa A. Uterine expression of prostaglandin H2 synthase in late pregnancy and during parturition in prostaglandin F receptor-deficient mice. Endocrinology 2000; 141:315–324.

21. Tsafriri A, Chun SY, Reich R. Follicular rupture and ovulation. In: Adashi EY, Leung PCK (eds.), The Ovary. New York: Raven Press; 1993: 227–244.
22. Tjandrawinata RR, Hughes-Fulford M. Up-regulation of cyclooxygenase-2 by product-prostaglandin E_2. Adv Exp Med Biol 1997; 407: 163–170.
23. Segi E, Sugimoto Y, Yamasaki A, Aze Y, Oida H, Nishimura T, Murata T, Matsuoka T, Ushikubi F, Hirose M, Tanaka T, Yoshida N, Narumiya S, Ichikawa A. Patent ductus arteriosus and neonatal death in prostaglandin receptor EP4-deficient mice. Biochem Biophys Res Commun 1998; 246:7–12.
24. Reich R, Daphna-Iken D, Chun SY, Popliker M, Slager R, Adelmann-Grill BC, Tsafriri A. Preovulatory changes in ovarian expression of collagenases and tissue metalloprotease inhibitor messenger ribonucleic acid: role of eicosanoids. Endocrinology 1991; 129:1869–1875.
25. Murdoch WH, Peterson TA, Van Kirk EA, Vincent DL, Inskeep EK. Interactive roles of progesterone, prostaglandins, and collagenase in the ovulatory mechanism of the ewe. Biol Reprod 1986; 35:1187–1194.
26. Miyaura C, Inada M, Suzawa T, Sugimoto Y, Ushikubi F, Ichikawa A, Narumiya S, Suda T. Impaired bone resorption to prostaglandin E_2 in prostaglandin E receptor EP4-knockout mice. J Biol Chem 2000; 275:19819–19823.
27. Sirois J. Induction of prostaglandin endoperoxide synthase-2 by human chorionic gonadotropin in bovine preovulatory follicles in vivo. Endocrinology 1994; 135:841–848.
28. Joyce IM, Pendola FL, O'Brien M, Eppig JJ. Regulation of prostaglandin-endoperoxide synthase 2 messenger ribonucleic acid expression in mouse granulosa cells during ovulation. Endocrinology 2001; 142:3187–3197.
29. Ando M, Kol S, Kakia E, Ruutiainen-Altman K, Sirois J, Rohan RM, Payne DW, Adashi EY. Rat ovarian prostaglandin endoperoxide synthase-1 and -2: preovulatory expression of granulosa cell-based interleukin-1-dependent enzymes. Endocrinology 1998; 139:2501–2508.
30. Chernaeva L, Charakchiva S. Estradiol effect on indomethacin and prostaglandin E_2-modulation of adrenergic transmission in rabbit oviduct. Prostaglandins 1991; 41:571–583.
31. Ortega-Moreno J. Influence of prostaglandins E_2 and F_2 alpha on passage pressure across the uterotubal junction and isthmus in the rat. Lab Anim 1995; 29:327–334.
32. Gawronska B, Paukku T, Huhtaniemi I, Wasowicz G, Ziecik A. Oestrogen-dependent expression of LH/hCG receptors in pig Fallopian tube and their role in relaxation of the oviduct. J Reprod Fertil 1999; 115:293–301.
33. Brenner RB, Slayden OD. Cyclic changes in the primate oviduct and endometrium. In: Knobil E, Neill JD (eds.), The Physiology of Reproduction, vol. 1, 2nd ed. New York: Raven Press; 1994: 541–569.
34. Verdugo P, Rumery RE, Tam PY. Hormonal control of oviductal ciliary activity: effect of prostaglandins. Fertil Steril 1980; 33:193–196.
35. Belley A, Chadee K. Prostaglandin E_2 stimulates rat and human colonic mucin exocytosis via the EP4 receptor. Gastroenterology 1999; 117:1352–1362.
36. Verrotti AC, Strickland S. Oocyte selection of mutation affecting cytoplasmic polyadenylation of maternal mRNAs. Mol Reprod Dev 1997; 46:482–488.

THE JOURNAL OF BIOLOGICAL CHEMISTRY
Vol. 278, No. 20, Issue of May 16, pp. 17977–17981, 2003
Printed in U.S.A.

Induction of Adherent Activity in Mastocytoma P-815 Cells by the Cooperation of Two Prostaglandin E_2 Receptor Subtypes, EP3 and EP4*

Received for publication, February 6, 2003, and in revised form, March 7, 2003
Published, JBC Papers in Press, March 11, 2003, DOI 10.1074/jbc.M301312200

Noriyuki Hatae, Ayumi Kita, Satoshi Tanaka, Yukihiko Sugimoto, and Atsushi Ichikawa‡

From the Department of Physiological Chemistry, Graduate School of Pharmaceutical Sciences, Kyoto University, Yoshida, Sakyo-ku, Kyoto 606, Japan

In this study, we investigated the role of PGE_2 in mouse mastocytoma P-815 cell adhesion to extracellular matrix proteins (ECMs) *in vitro*. We report that PGE_2 accelerated ProNectin F™ (a proteolytic fragment of fibronectin)-mediated adhesion, which was abolished by addition of the GRGDS peptide, an inhibitor of the RDG binding site of ProNectin F™. We show that the cAMP level and cAMP-regulated protein kinase (PKA) activity are critical mediators of this PGE_2 effect, because the cell-permeable cAMP analogue 8-Br-cAMP accelerated P-815 cell adhesion to ProNectin F™ and the pharmacological inhibitor of PKA, H-89, blocked PGE_2-mediated adhesion. Consistent with mRNA expression of the G_s-coupled EP4- and G_i-coupled EP3-PGE receptor subtypes, P-815 cell adhesion was accelerated by treatment with a selective EP4 agonist, ONO-AE1-329, but not a selective EP1/EP3 agonist, sulprostone. However, simultaneous treatment with ONO-AE1-329 and sulprostone resulted in augmentation of both the cAMP level and cell adhesion. The augmentation of EP3-mediated cAMP synthesis was dose-dependent, without affecting the half-maximal concentration for EP4-mediated G_s-activity, which was inhibited by a G_i inhibitor, pertussis toxin. In conclusion, these findings suggest that PGE_2 accelerates RGD-dependent adhesion via cooperative activation between EP3 and EP4 and contributes to the recruitment of mast cells to the ECM during inflammation.

Differentiated mast cells (MCs),[1] which originate from bone marrow stem cells, traffic throughout the circulation and adhere to the extracellular matrix (ECM) in various tissues. MCs are widely distributed in tissues throughout the body, especially in connective tissues, serosal cavities, and on mucosal surfaces under normal physiological conditions. This characteristic distinguishes MCs from other bone marrow-derived hematopoietic cells, such as basophils, neutrophils, and eosinophils. MCs congregate around nerves, blood vessels, and lymphatic vessels. MCs therefore interact with not only the ECM but with other cells as well. As well known for rodent connective tissue-typed MCs and mucosal-typed MCs, the biological activity of MCs vary with their interactions with the ECM and other cells.

MCs are widely distributed along basement membranes, indicating that MCs might adhere to laminin. Supporting this fact, mouse bone marrow-derived mast cells (BMMC) have been reported to adhere to laminin, when the cells were activated by phorbol 12-myristate 13-acetate (PMA) (1–3) or antigen-stimulated aggregation of FcεRI (4). In addition to laminin, MCs can adhere to other matrix components such as fibronectin (5) and vitronectin (6, 7). As with laminin, the adherence of BMMC to fibronectin has been reported to occur through activation with PMA or after aggregation of FcεRI. These adherence activities required calcium (3). In contrast to BMMC, the mouse PT18 cell line spontaneously adhered to laminin (1), and human skin mast cells also spontaneously adhered to laminin and fibronectin (8). These previous findings indicate that the interactions between MCs and matrix components may depend on the cells involved and the kinds of stimuli.

PGE_2, which is involved in inflammation section (9), affects both differentiation and growth of MCs *in vitro*. PGE_2 enhances mast cell differentiation from cord blood mononuclear cells (10) and in the fibroblast co-culture system (11). Very recently, Dormond *et al.* (12) reported that a COX-2 inhibitor suppressed $\alpha_V\beta_3$-dependent HUVEC spreading, migration, and angiogenesis through Rac activation (12), and PGE_2 accelerated $\alpha V\beta 3$-mediated HUVEC responses in a cAMP-dependent manner (13). However, no reports have published the effects of PGE_2 on MC adhesion to the ECM.

The PGE_2 receptors (EP) are comprised of four subtypes, EP1, EP2, EP3, and EP4, which are coupled to different G proteins and signal pathways (14, 15). Among these subtypes, EP2 and EP4 couple to G_s, resulting in increases of intracellular cAMP concentrations (16, 17), while EP3 couples to G_i, causing a decrease in cAMP levels (18–21). Very recently, we and other investigators have reported that activation of the G_i-coupled EP3 receptor was able to augment adenylyl cyclase activity via stimulation of a G_s-coupled receptor (22, 23). We previously reported that the mouse EP3β receptor was able to augment EP2-induced adenylyl cyclase activity in both EP2- and EP3-transfected COS-7 cells (22). Southall and Vasko (23) showed that the simultaneous depletion of rat EP3C and EP4 was essential to abolish PGE_2-stimulated cAMP production and neuropeptide release in rat sensory neurons (23). These permissive actions between the two subtypes may be involved in the events of a number of physiological actions of PGE_2 (15).

* This work was supported in part by a grant-in-aid for Scientific Research by the Ministry of Education, Science, Sports, and Culture of Japan. The costs of publication of this article were defrayed in part by the payment of page charges. This article must therefore be hereby marked "*advertisement*" in accordance with 18 U.S.C. Section 1734 solely to indicate this fact.

‡ To whom correspondence should be addressed: Dept. of Physiological Chemistry, Faculty of Pharmaceutical Sciences, Kyoto University, Sakyo-ku, Kyoto 606, Japan. Tel.: 81-75-753-4527; Fax: 81-75-753-4557; E-mail: aichikaw@pharm.kyoto-u.ac.jp.

[1] The abbreviations used are: MC, mast cell; PG, prostaglandin; G protein, heterotrimeric GTP-binding protein; PT, pertussis toxin; PMA, phorbol 12-myristate 13-acetate; PBS, phosphate-buffered saline; Mes, 4-morpholineethanesulfonic acid; PI3K, phosphatidylinositol 3-kinase; PKA, cAMP-dependent protein kinase; ECM, extracellular matrix.

Here we extended the analyses of the effects of PGE_2 on adhesion of mouse mastocytoma P-815 cells to the fibronectin component in a PKA-dependent manner, and we examined the correlation between cAMP levels and adhesion in P-815 cells to see whether EP3 could augment EP4-induced cAMP synthesis.

EXPERIMENTAL PROCEDURES

Materials—Sulprostone was a generous gift from Dr. M. P. L. Caton of Rhone-Poulenc Ltd. ONO-AE1-259 and ONO-AE1-329 were generous gifts from ONO Pharmaceuticals (Osaka, Japan). ProNectin F™ (Pronectin-F) and ProNectin L™ (Pronectin-L) were generous gifts from Sanyo Chemical Industries, Ltd. (Kyoto, Japan). The GRGDS peptide was obtained from the PEPTIDE Institute (Osaka, Japan). Collagen I-coated plates were from BD PharMingen Labware, the ^{125}I-labeled cAMP assay system from Amersham Biosciences. Pertussis toxin (PT) from Seikagaku Kogyo (Tokyo, Japan), [5,6,8,11,12,14,15-^{3}H]PGE_2 (164 Ci/mmol) from Amersham Biosciences and PGE_2 from Cayman Chemical (Ann Arbor, MI). Rabbit polyclonal anti-A cyclase II (C-20) antibody, rabbit polyclonal anti-A cyclase IV (C-20) antibody, and goat polyclonal anti-A cyclase VII (M-20) antibody were obtained from Santa Cruz Biotechnology (Santa Cruz, CA).

Reverse Transcription-Polymerase Chain Reaction—Mouse mastocytoma P-815 cells (P-815 cells) were maintained in Fischer's medium with 10% fetal bovine serum under humidified air containing 5% CO_2 at 37 °C. Total RNA was isolated from P-815 cells using Isogen (Nippon Gene) according to the manufacturer's instructions. The reverse transcription (RT) reaction was performed using Molony murine leukemia virus reverse transcriptase (Invitrogen) in the presence of random hexamers. The polymerase chain reaction (PCR) was performed with *Taq* DNA polymerase (TOYOBO) using the first strand template. The primers were designed to be selective for the prostanoid receptors, and the sequences used were as follows: EP1 (base pairs (545 bp)), 5′-GCC ACT GAT CCA CGC GGC GCG CGT ATC TGT GGC C-3′ (forward) and 5′-CGA TGG CCA ACA CCA CCA ACA CCA GCA GGG-3′ (reverse); EP2 (604 bp), 5′-TTC ATA TTC AAG AAA CCA GAC CCT GGT GGC-3′ (forward) and 5′-AGG GAA GAG GTT TCA TCC ATG TAG GCA AAG-3′ (reverse); EP3 (608 bp), 5′-ATC CTC GTG TAC CTG TCA CAG CGA CGC TGG-3′ (forward) and 5′-TGC TCA ACC GAC ATC TGA TTG AAG ATC ATT-3′ (reverse); EP4 (601 bp), 5′-GAC TGG ACC ACC AAC GTA ACG GCC TAC GCC-3′ (forward) and 5′-ATG TCC TCC GAC TCT CTG AGC AGT GCT GGG-3′ (reverse); IP (602 bp), 5′-CCT GCA GTG TTT GTG GCC TAT GCT CGA AAC-3′ (forward) and 5′-CTG CTG TCT GGG GCG ATG GCC TGA GTG AAG-3′ (reverse); DP (604 bp), 5′-AAA GGA ACT GCT GCC TGC CTC AGG CAA TCA-3′ (forward) and 5′-GTT CTC AAG TTT AAA GGC TCC ATA GTA CGC-3′ (reverse); FP (603 bp), 5′-GCA TAG CTG TCT TTG TAT ATG CTT CTG ATA-3′ (forward) and 5′-GTG TCG TTT CAC AGG TCA CTG GGG AAT TAT-3′ (reverse); TP (607 bp), 5′-TGC CTT GTT GGA CTG GCG AGC CAC TGA CCC-3′ (forward) and 5′-CAG GTA GAT GAG CAG CTG GTG CTC TGT GGC-3′ (reverse). The thermal cycle programs used were as follows: EP1, 94 °C for 1 min and then 94 °C for 1 min, 72 °C for 3.5 min for the first 10 cycles, 94 °C for 1 min, 69 °C for 2 min, 72 °C for 1.5 min for the next 10 cycles, 94 °C for 1 min, 66 °C for 2 min, 72 °C for 1.5 min for the last 15 cycles, followed by 72 °C for 7 min; EP2, EP3, EP4 and DP, 94 °C for 1 min and then 30 cycles of 94 °C for 0.8 min, 60 °C for 0.7 min, 72 °C for 1.5 min, followed by 72 °C for 7 min; IP, 94 °C for 1 min and then 30 cycles of 94 °C for 0.8 min, 65 °C for 0.7 min, 72 °C for 1.5 min, followed by 72 °C for 7 min; FP and TP, 94 °C for 1 min and then 94 °C for 1 min, 72 °C for 3.5 min for the first 10 cycles, 94 °C for 1 min, 67 °C for 2 min, 72 °C for 1.5 min for the next 10 cycles, 94 °C for 1 min, 63 °C for 2 min, 72 °C for 1.5 min for the last 15 cycles, followed by 72 °C for 7 min. Samples were visualized on a 1.5% agarose gel.

[^{3}H]PGE_2 Binding Assay—P-815 cells were homogenized with a Potter-Elvehjem homogenizer in 20 mM Tris-HCl (pH 7.5), containing 10 mM $MgCl_2$, 1 mM EDTA, 20 μM indomethacin, and 0.2 mM phenylmethylsulfonyl fluoride. After centrifugation at 250,000 × *g* for 20 min, the pellet (membrane fraction) was washed, suspended in 10 mM Mes-NaOH (pH 6.0) containing 10 mM $MgCl_2$, and 1 mM EDTA, and was used for the [^{3}H]PGE_2 binding assay. The membrane fraction (50 μg) was incubated with 4 nM [^{3}H]PGE_2 at 30 °C for 1 h, and [^{3}H]PGE_2 binding to the membrane fraction was determined as described previously (24). Nonspecific binding was determined using a 2,500-fold excess of unlabeled PGE_2 in the incubation mixture.

Measurement of cAMP Formation—Cyclic AMP levels in P-815 cells were determined as reported previously (25). P-815 cells (2×10^6 cells/assay) were suspended with 10 μM indomethacin in HEPES-buffered saline containing 140 mM NaCl, 4.7 mM KCl, 2.2 mM $CaCl_2$, 1.2 mM $MgCl_2$, 1.2 mM KH_2PO_4, 11 mM glucose, and 15 mM HEPES (pH 7.4), and preincubated for 10 min at 37 °C. Reactions were started by addition of test agents along with 500 μM 3-isobutyl-1-methyl-xanthine (Sigma). After incubation for 10 min at 37 °C, reactions were terminated by the addition of 10% trichloroacetic acid. The level of cAMP was measured by radioimmunoassay with an Amersham Biosciences cAMP assay system.

Expression of the Adenylyl Cyclase Subtypes—Expression of adenylyl cyclase II, IV, and VII were determined by immunoblot analysis of whole cell detergent lysates of P-815 cells using rabbit polyclonal anti-A cyclase II (C-20) antibody, rabbit polyclonal anti-A-cyclase IV (C-20) antibody, and goat polyclonal anti-A cyclase (M-20) antibody. P-815 cells (2×10^8 cells) were washed twice in PBS. The cell pellet was suspended in 1 ml of radioimmune precipitation assay buffer containing 30 mM HEPES-NaOH (pH 7.3), 150 mM NaCl, 1% Triton X-100, 1% deoxycholate, and 0.1% SDS, and incubated for 2 h at 4 °C. For protection against proteolytic degradation, a mixture of protease inhibitors (0.2 mM phenylmethylsulfonyl fluoride, 100 μM benzamidine, 10 μg/ml leupeptin, 10 μg/ml aprotinin, 10 μg/ml E-64, and 1 μg/ml pepstatin A) was added. The mixture was then centrifuged at 10,000 × *g* for 15 min at 4 °C. The resulting supernatant was dissolved in Laemmli buffer and heated for 30 min at 60 °C. Aliquots (500 μg of protein) were then subjected to SDS-PAGE (7.5%) as described by Laemmli (26), and the separated proteins were transferred electrophoretically onto a polyvinylidene difluoride membrane in 25 mM Tris base containing 40 mM 6-aminohexanoic acid, 0.02% SDS, and 20% methanol at room temperature for 30 min at 15 V. The membrane fraction was rinsed in Tris-buffered saline (TBS) containing 20 mM Tris-HCl (pH 7.5) and 150 mM NaCl, and then preincubated overnight in TBS containing 5% nonfat milk at 4 °C. The membrane fraction was then incubated with anti-A cyclase antibodies (A cyclase II, IV, 1:200; A cyclase VII, 1:100) in TBS containing 5% nonfat milk for 1 h at 37 °C. After washing three times with TTBS (TBS containing 0.05% Tween 20) at room temperature, the membrane fraction was incubated with peroxidase-conjugated anti-rabbit or -goat IgG in TTBS for 1 h at room temperature, and then detected with the ECL Western blot detection reagent.

Cell Adhesion Assay—P-815 cells were suspended in Fischer's medium with test agents along with 10% fetal bovine serum and 10 μM indomethacin at a density of 5×10^5 cells per ml, and 1 ml per well was dispensed into 12-well tissue culture plates. The 12-well tissue culture plates were precoated with 10 μg/ml of Pronectin-F or Pronectin-L for 5 min at room temperature. Nonspecific binding was determined by using wells precoated with bovine serum albumin (3%) for 1 h at room temperature. The P-815 cells were incubated for 8 h at 37 °C in a CO_2-humidified atmosphere and non-adherent P-815 cells were suspended in 2 ml of PBS (non-adherent cells). The adherent P-815 cells were treated with PBS containing 0.02% EDTA and 0.25% trypsin at 37 °C for 30 min, and the collected cells were suspended in 2 ml of PBS containing 0.02% EDTA and 2% fetal bovine serum (adherent cells). The numbers of non-adherent and adherent cells were counted using the COULTER Z1 cell counter (Beckman Coulter). The percentage of cell adhesion was calculated with the following formula shown in Equation 1.

$$\% \text{ cell adhesion} = \text{adherent cell number} \times 100/(\text{adherent cell number} + \text{non-adherent cell number}) \quad \text{(Eq. 1)}$$

RESULTS

P-815 Cell Adhesion to Pronectin-F-coated Plates—When P-815 cells were cultured in Fischer's medium containing 10% fetal bovine serum together with 10 μM indomethacin, almost no attachment to non-coated plates was observed. However, after incubation with 1 μM PGE_2 for 8 h, ~11% of P-815 cells were retained on the non-coated plates as adhered cells, after being washed three times with PBS containing 0.02% EDTA (Fig. 1*A*). We next examined the effect of fibronectin on cell adhesion using Pronectin-F, which consists of multiple copies of the RGD cell attachment ligand of fibronectin (27). The number of adhered P-815 cells did not significantly change between the Pronectin-F-coated plates and the non-coated plates when the cells were incubated without PGE_2, but markedly increased upon incubation with 1 μM PGE_2 (Fig. 1*B*). PGE_2-induced adherent activity to Pronectin-F-coated plates

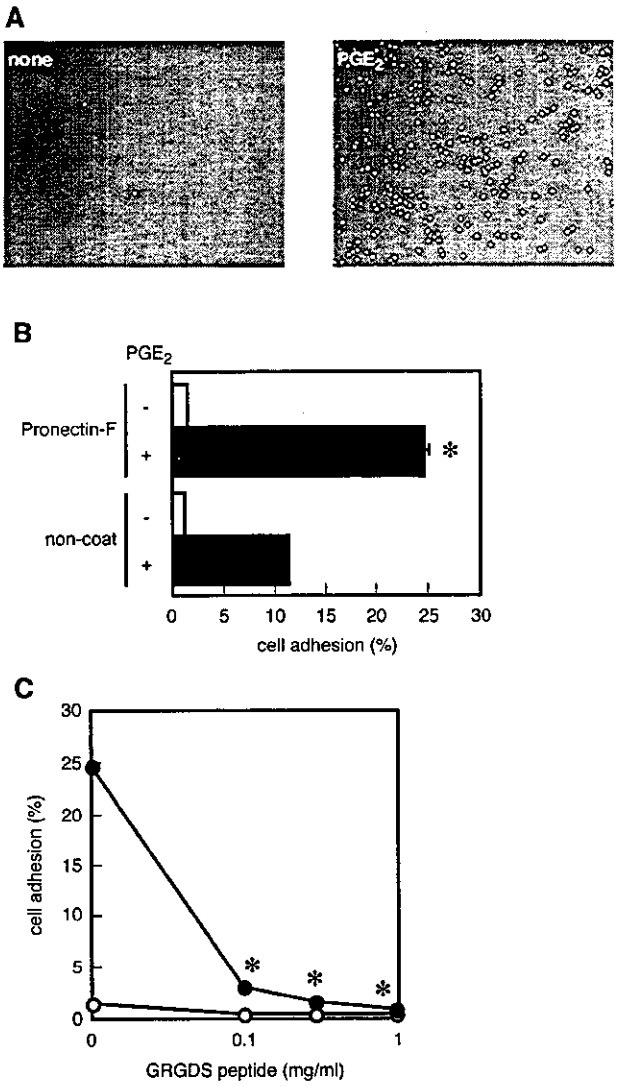

FIG. 1. **Adhesion of PGE_2-stimulated P-815 cells to Pronectin-F-coated plates.** *A*, P-815 cells were incubated at 37 °C for 8 h with or without 1 μM PGE_2. *B*, P-815 cells were incubated at 37 °C for 8 h in wells coated with or without Pronectin-F (10 μg/ml) in the presence (*solid bars*) or absence (*open bars*) of 1 μM PGE_2, and the percentages of P-815 cell adhesion were determined as described under "Experimental Procedures." Values are shown as the means ± S.E. of triplicate experiments. *, $p < 0.01$ *versus* non-coat. *C*, P-815 cells were incubated at 37 °C for 8 h in wells coated with Pronectin-F (10 μg/ml) in the presence (*closed circles*) or absence (*open circles*) of 1 μM PGE_2 together with the indicated concentrations of soluble GRGDS peptide, and the percentages of P-815 cell adhesion were determined as described under "Experimental Procedures." Values are means ± S.E. for triplicate experiments. *, $p < 0.01$ *versus* without the GRGDS peptide.

almost completely disappeared with addition of the GRGDS peptide (Fig. 1*C*), which is a soluble inhibitor for the RDG site of fibronectin as well as Pronectin-F (28). Furthermore, this PGE_2-treated cell adhesion was not affected by further incubation with 0.02% EDTA for 30 min, but the cells could be detached by 0.25% trypsin treatment.

Expression of the EP3 and EP4 Subtypes in P-815 Cells—The RT-PCR experiment revealed that P-815 cells express mRNAs for EP3, EP4, and IP (Fig. 2*A*). We confirmed the expression of the EP3 and EP4 receptor proteins by the replacement of the binding of 4 nM [^{3}H]PGE_2 to membrane fractions with 10 μM PGE_2, sulprostone (EP1 and EP3 agonist), or ONO-AE1–329 (EP4 agonist). The order of replacement potency was found to be PGE_2 > sulprostone > ONO-AE1–329 (Fig. 2*B*). These results indicate that PGE_2 can bind to EP3 and EP4 present in the membrane fractions of P-815 cells.

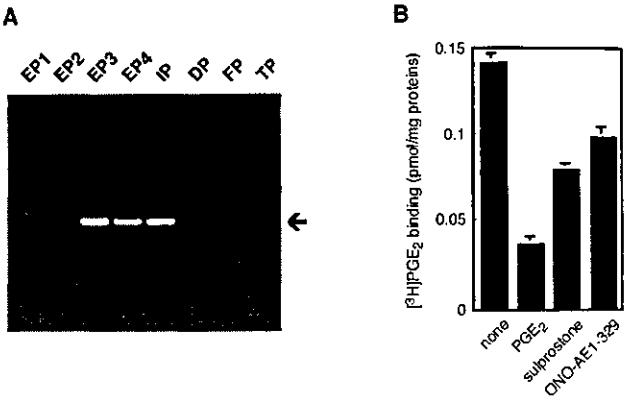

FIG. 2. **Detection of prostaglandin receptor mRNAs and prostaglandin E_2 receptor subtype proteins in P-815 cells.** *A*, expression of mRNAs for the prostanoid receptors was assessed by RT-PCR. Total RNA from P-815 cells was isolated and subjected to RT-PCR, and PCR products for the EP1, EP2, EP3, EP4, IP, DP, FP, and TP receptors were detected according to the procedures described under "Experimental Procedures." *B*, expression of the EP subtypes, EP3 and EP4, was assessed by [^{3}H]PGE_2 binding to each subtype. The membranes of P-815 cells were incubated at 30 °C for 1 h with 4 nM [^{3}H]PGE_2 in the presence or absence (none) of 10 μM PGE_2, 0.1 μM sulprostone (EP1, 3 agonist), 0.1 μM ONO-AE1–329 (EP4 agonist). Values are the means ± S.E. for triplicate determinations.

PGE_2-induced cAMP and Protein Kinase A-dependent P-815 Cell Adhesion—Along with PGE_2, 8-Br-cAMP, and IBMX accelerated the adhesion of P-815 cells to Pronectin-F-coated plates (Fig. 3*A*). PGE_2-mediated cell adhesion was greatly reduced by pretreatment with 10 μM H-89, a PKA inhibitor (Fig. 3*B*). On the other hand, phorbol 12-myristate 13-acetate (PMA) had no effect on cell adhesion in the absence of PGE_2, and in addition, PGE_2 did not change the intracellular Ca^{2+} level (data not shown). These results suggest that the PGE_2-induced adhesion of P-815 cells to Pronectin-F is via a cAMP-dependent and cAMP-protein kinase A-dependent pathway.

Sulprostone-induced Augmentation of ONO-AE1–329-induced cAMP Formation in P-815 Cells—Since P-815 cells express the G_i-coupled EP3 as well as the G_s-coupled EP4, it is possible that PGE_2 may bind to both subtype receptors at the same time, and hence the cAMP level may reflect the difference between G_s- and G_i-activated adenylyl cyclase activity. We therefore examined the cAMP levels in P-815 cells when treated with the EP1/EP3 agonist sulprostone and/or the EP4 agonist ONO AE1–329 (Fig. 4*A*). The cAMP level was increased by treatment with ONO-AE1–329 and reached a plateau level at 0.1 μM. However, cAMP accumulation induced by various concentrations of the EP4 agonist were all augmented by the simultaneous addition of sulprostone (1 μM), without affecting the half-maximal concentration, although sulprostone alone did not stimulate cAMP accumulation (Fig. 4*A*). The half-maximal concentration of sulprostone for EP3-mediated augmentation in EP4-induced cAMP synthesis was calculated to be $\sim 5 \times 10^{-8}$ M (data not shown). Furthermore, sulprostone-induced augmentation of ONO-AE1–329-activated cAMP formation was absolutely inhibited by treatment with PT, and the cAMP level was almost equal to that observed in the cells stimulated by ONO-AE1–329 alone (Fig. 4*B*). These findings suggest that EP3-mediated augmentation of G_s activity is achieved through $G\beta\gamma$ subunits resulting from $G_{i/o}$ protein activation (29), although EP4-mediated G_s activity is not.

Sulprostone-induced Augmentation of ONO-AE1–329-stimulated P-815 Cell Adhesion to Pronectin-F—We next examined whether EP3 stimulation could augment EP4-mediated adhe-

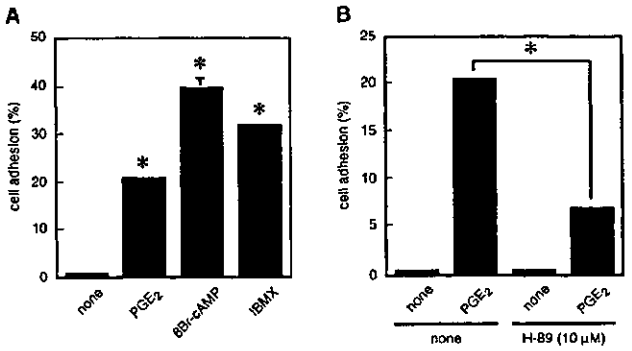

FIG. 3. **Adhesion of PGE_2-stimulated P-815 cells to Pronectin-F-coated wells mediated by PKA activation.** *A*, P-815 cells were incubated at 37 °C for 8 h in wells coated with Pronectin-F (10 μg/ml) in the presence of 1 μM PGE_2, 1 mM 8Br-cAMP, or 0.5 mM IBMX, and the percentages of P-815 cell adhesion were determined as described under "Experimental Procedures." Values are shown as the means ± S.E. for triplicate experiments. *, $p < 0.01$ *versus* untreated. *B*, P-815 cells were preloaded with or without 10 μM H-89 for 30 min, then the cells were incubated for 8 h in the presence or absence of 1 μM PGE_2, with or without 10 μM H-89. The percentages of P-815 cell adhesion were determined as described under "Experimental Procedures." Values are shown as the means ± S.E. for triplicate experiments. *, $p < 0.01$ *versus* without H-89 treatment.

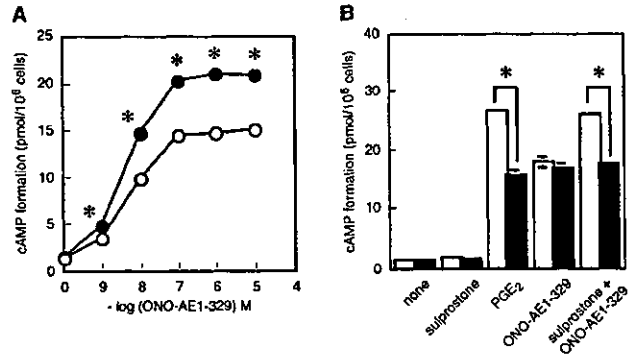

FIG. 4. **Sulprostone-induced augmentation of ONO-AE1-329-stimulated cAMP formation in P-815 cells.** *A*, P-815 cells were incubated at 37 °C for 10 min with 1 μM sulprostone in the presence of indicated concentrations of ONO-AE1-329. cAMP formation was determined as described under "Experimental Procedures." Values are the means ± S.E. of triplicate experiments. *, $p < 0.01$ *versus* stimulation with the indicated concentrations of ONO-AE1-329 alone. *B*, P-815 cells were pretreated with 25 ng/ml PT for 7 h, and the treated cells were then incubated at 37 °C for 10 min with 1 μM PGE_2, 1 μM sulprostone, 1 μM ONO-AE1-329, or both 1 μM sulprostone and 1 μM ONO-AE1-329, and cAMP formation was determined as described under "Experimental Procedures." Values are shown as the means ± S.E. for triplicate experiments. *, $p < 0.01$ *versus* without PT treatment.

sion of P-815 cells to Pronectin-F. 1 μM sulprostone further augmented ONO-AE1-329 induced P-815 cell adhesion to Pronectin-F (Fig. 5), and the level of EP3-mediated augmentation of this adhesion was almost equal to the level of cAMP augmentation by the EP3 subtype (Fig. 4*B*). These findings suggest that PGE_2-stimulated P-815 cell adhesion to Pronectin-F is mediated through the cooperative action of the EP3 and EP4 subtypes.

DISCUSSION

PGE_2 was previously reported to affect both differentiation and growth of mast cells *in vitro*. For example, PGE_2 is essential for the differentiation of IL-3-dependent mouse mast cells from spleen cells (30), PGE_2 enhanced human mast cell differentiation from cord blood mononuclear cells by inhibiting the production of macrophage-derived GM-CSF (10), and PGE_2 enhanced the growth of differentiated mast cells in a fibroblast

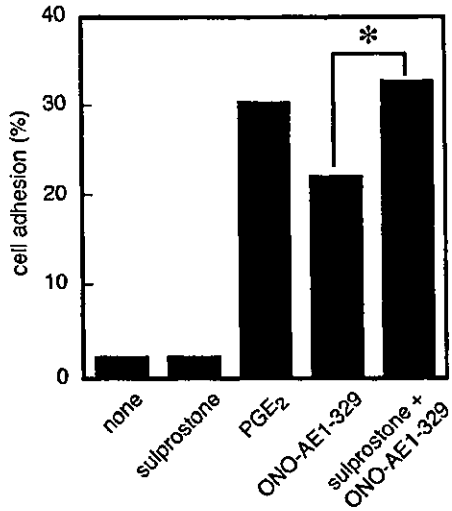

FIG. 5. **Effect of PGE_2 on adhesion of P-815 cells to Pronectin-F-coated wells.** P-815 cells were incubated at 37 °C for 8 h in wells coated with Pronectin-F (10 μg/ml) in the presence or absence of 1 μM PGE_2, 1 μM sulprostone, 1 μM ONO-AE1-329, or both 1 μM sulprostone and 1 μM ONO-AE1-329. The percentages of P-815 cell adhesion were determined as described under "Experimental Procedures." Values are shown as the means ± S.E. for triplicate experiments. *, $p < 0.01$ *versus* stimulation with ONO-AE1-329 alone.

co-culture system (11). It is therefore possible that PGE_2 plays a role in the interaction of mast cells with fibroblastic cells and extracellular matrix components. The interaction between mast cells and extracellular matrix components have profound influences on the targeting of mast cell progenitors to specific locations, the distribution of mast cell subsets, and the biological responsiveness of mast cells in tissues. The ability of mast cells to adhere to fibronectin, which involves the RGD sequence located within the cell-attachment domain of the fibronectin molecule, may play a role in the migration of mast cells in various tissues (5). In the present report, we found that PGE_2 is able to stimulate the adhesion of P-815 cells to Pronectin-F through the RGD cell attachment domain of fibronectin, and that this adherent activity is mediated via a cAMP-dependent pathway induced by the activation of the EP4 and/or EP3 receptors. It is possible that the cAMP-protein kinase A pathway may be involved in the induction of these cell attachment molecules, as PGE_2-induced cell attachment was inhibited by treatment with H-89 (Fig. 3*B*) and cycloheximide (data not shown). However, neither PGE_2 nor 8Br-cAMP augmented the expression of VLA-5, one of the fibronectin receptors (data not shown). Therefore, cycloheximide may affect the signaling pathway of the fibronectin receptors. Further experiments are required to clarify these points.

Prostaglandin E_2 acts through binding to its specific receptors, which are comprised of four subtypes, EP1, EP2, EP3, and EP4 (14, 15). Among them, EP3 and EP4 couple to G_i and G_s, and result in inhibition and stimulation of adenylyl cyclase activity, respectively (17–21). The mouse EP3 receptor is comprised of three isoforms, EP3α, EP3β, and EP3γ, which differ in their C terminus. Among them, EP3β, which was used in this experiment is known to be coupled to the G_i protein (19). Very recently, activation of a G_i-coupled receptor has been reported to augment the adenylyl cyclase activity induced by the stimulation of a G_s-coupled receptor in COS-7 cells. For example, activation of G_i-coupled receptors such as α2 adrenoreceptor (29) and bradykinin B2 receptor (32) lead to the augmentation of G_s-stimulated adenylyl cyclase in COS-7 cells. This synergistic effect has not been clearly shown in mammalian cells. Southall and Vasko (23) showed that the simultaneous deple-

tion of both rat EP3C and EP4 was essential for abolishing PGE_2-stimulated cAMP production and neuropeptide release in rat sensory neurons (23). In the current experiment we showed that the G_i-coupled EP3 agonist sulprostone augmented cAMP formation induced by the EP4 agonist ONO-AE1-329 in P-815 cells. Similarly, we found that sulprostone was able to augment cAMP formation in P-815 cells activated by an IP agonist, carbacyclin, suggesting that the augmentative effects of EP3 can be observed irrespective of G_s activation. The mechanism underlying these phenomena was thought to be via $G\beta\gamma$-mediated activation of type IV adenylyl cyclase (29), because pretreatment with PT inhibited the augmentation by the activation of the G_i-coupled EP3 receptor, and P-815 cells express type IV adenylyl cyclase (data not shown). Therefore, $G\beta\gamma$-mediated activation of type IV adenylyl cyclase may be involved in EP3-mediated signaling to augment EP4-stimulated adenylyl cyclase activity in P-815 cells.

Although the involvement of phosphatidylinositol 3-kinase (PI3K) in cell adhesion to matrix proteins is shown in a variety of cell types (33), the role of PI3K in mast cell adhesion is still unknown. Kinashi *et al.* (31) reported that the adhesion of platelet-derived growth factor receptor-expressed bone marrow-derived mast cells was inhibited by the addition of the PI3K inhibitor wortmannin. To understand whether PI3K is activated by PGE_2 during P-815 cell adhesion, we examined the effect of the PI3K inhibitors, wortmannin (100 nM) and LY294002 (10 μM) on EP3/EP4-agonist induced cell adhesion to fibronectin. As a result, these inhibitors showed an additive effect on the augmentation of PGE_2-induced cell adhesion (wortmannin: 81.7 ± 0.1% and LY294002: 82.4 ± 0.2%, compared with PGE_2 stimulation alone: 24.8 ± 0.6%). Furthermore, each inhibitor alone had an effect on cell adhesion (wortmannin: 20.4 ± 0.1% and LY294002: 24.1 ± 0.1%, compared with the absence of these inhibitors (3.3 ± 0.1%)). Therefore, these results indicate that P-815 cell attachment to fibronectin is regulated by two independent signaling pathways involving PKA and PI3K. Further experiments are necessary to clarify the fundamental differences in the signaling involving PKA and PI3K in P-815 cell attachment to fibronectin. In summary, this study clearly demonstrates that two subtypes of the PGE_2 receptor, EP3 and EP4, are cooperatively involved in PGE_2-evoked and cAMP-mediated functions of P-815 cell adhesion.

Acknowledgments—We thank Dr. M. P. L. Caton of Rhone-Poulenc Ltd. for the generous gift of sulprostone. We are grateful to Dr. Manabu Negishi of the Laboratory of Molecular Neurobiology, Graduate School of Biostudies, University of Kyoto for valuable advice on this study.

REFERENCES

1. Thompson, H. L., Burbelo, P. D., Segui-Real, B., Yamada, Y., and Metcalfe, D. D. (1989) *J. Immunol.* **143,** 2323–2327
2. Thompson, H. L., Burbelo, P. D., Yamada, Y., Kleiman, H. K., and Metcalfe, D. D. (1989) *J. Immunol.* **143,** 4188–4192
3. Thompson, H. L., Burbelo, P. D., Yamada, Y., Kleiman, H. K., and Metcalfe, D. D. (1991) *Immunology* **72,** 144–149
4. Thompson, H. L., Burbelo, P. D., and Metcalfe, D. D. (1990) *J. Immunol.* **145,** 3425–3431
5. Dastych, J., Costa, J. J., Thompson, H. L., and Metcalfe, D. D. (1991) *Immunology* **73,** 478–484
6. Bianchine, P. J., Burd, P. R., and Metcalfe, D. D. (1992) *J. Immunol.* **149,** 3665–3671
7. Gurish, M. F., Bell, A. F., Smith, T. J., Ducharme, L. A., Wang, R.-K., and Weis, J. H. (149) *J. Immunol.* **149,** 1964–1972
8. Walsh, L. J., Kaminer, M. S., Lazarus, G. S., Lavker, R. M., and Murphy, G. F. (1991) *Lab. Invest.* **65,** 433–439
9. Ohuchi, K., Yoshino, S., Kanaoka, K., Tsurufuji, S., and Levine, L. (1982) *Int. Archs. Allergy Appl. Immun.* **68,** 326–331
10. Saito, H., Ebisawa, M., Tachimoto, H., Shichijo, M., Fukagawa, K., Matsumoto, K., Iikura, Y., Awaji, T., Tsujimoto, G., Yanagida, M., Uzumaki, H., Takahashi, G., Tsuji, K., and Nakahata, T. (1996) *J. Immunol.* **157,** 343–350
11. Kameyoshi, Y., Morita, E., Tanaka, T., Hiragun, T., and Yamamoto, S. (2000) *Arch. Dermatol. Res.* **292,** 240–247
12. Dormond, O., Foletti, A., Paroz, C., and Ruegg, C. (2001) *Nat. Med.* **7,** 1041–1047
13. Dormond, O., Bezzi, M., Mariotti, A., and Ruegg, C. (2002) *J. Biol. Chem.* **277,** 45838–45846
14. Coleman, R. A., Smith, W. L., and Narumiya, S. (1994) *Pharmacol. Rev.* **46,** 205–229
15. Narumiya, S., Sugimoto, Y., and Ushikubi, F. (1999) *Physiol. Rev.* **79,** 1193–1226
16. Katsuyama, M., Nishigaki, N., Sugimoto, Y., Morimoto, K., Negishi, M., Narumiya, S., and Ichikawa, A. (1995) *FEBS Lett.* **372,** 151–156
17. Honda, A., Sugimoto, Y., Namba, T., Watabe, A., Irie, A., Negishi, M., Narumiya, S., and Ichikawa, A. (1993) *J. Biol. Chem.* **268,** 7759–7762
18. Sugimoto, Y., Namba, T., Honda, A., Hayashi, Y., Negishi, M., Ichikawa, A., and Narumiya, S. (1992) *J. Biol. Chem.* **267,** 6463–6466
19. Sugimoto, Y., Negishi, M., Hayashi, Y., Namba, T., Honda, A., Watabe, A., Hirata, M., Narumiya, S., and Ichikawa, A. (1993) *J. Biol. Chem.* **268,** 2712–2718
20. Irie, A., Sugimoto, Y., Namba, T., Harazono, A., Honda, A., Watabe, A., Negishi, M., Narumiya, S., and Ichikawa, A. (1993) *Eur. J. Biochem.* **217,** 313–318
21. Irie, A., Segi, E., Sugimoto, Y., Ichikawa, A., and Negishi, M. (1994) *Biochem. Biophys. Res. Commun.* **204,** 303–309
22. Hatae, N., Yamaoka, K., Sugimoto, Y., Negishi, M., and Ichikawa, A. (2002) *Biochem. Biophys. Res. Commun.* **290,** 162–168
23. Southall, M. D., and Vasko, M. R. (2001) *J. Biol. Chem.* **276,** 16083–16091
24. Negishi, M., Irie, A., Sugimoto, Y., Namba, T., and Ichikawa, A. (1995) *J. Biol. Chem.* **270,** 16122–16127
25. Negishi, M., Sugimoto, Y., Irie, A., Narumiya, S., and Ichikawa, A. (1993) *J. Biol. Chem.* **268,** 9517–9521
26. Laemmli, U. K. (1970) *Nature* **227,** 680–685
27. Anderson, J. P., Cappello, J., and Martin, C. (1994) *Biopolymers* **34,** 1049–1057
28. Akiyama, S. K., and Yamada, K. M. (1985) *J. Biol. Chem.* **260,** 10402–10405
29. Fereman, A. D., Conklin, B. R., Schrader, K. A., Reed, R. R., and Bourne, H. R (1992) *Nature* **356,** 159–161
30. Hu, Z. Q., Asano, K., Seki, H., and Shimamura, T. (1995) *J. Immunol.* **15** 2134–2142
31. Kinashi, T., Escobedo, J. A., Williams, L. T., Takatsu, K., and Springer, T. (1995) *Blood* **86,** 2086–2090
32. Hanke, S., Nurnberg, B., Groll, D. H., and Liebmann, C. (2001) *Mol. Cell. Bi* **21,** 8452–8460
33. Wu, C. (1999) *J. Cell Sci.* **112,** 4485–4489

Host Prostaglandin E_2-EP3 Signaling Regulates Tumor-Associated Angiogenesis and Tumor Growth

Hideki Amano,[1,2] Izumi Hayashi,[1] Hirahito Endo,[3] Hidero Kitasato,[4] Shohei Yamashina,[5] Takayuki Maruyama,[6] Michiyoshi Kobayashi,[6] Kazutoyo Satoh,[6] Masami Narita,[6] Yukihiko Sugimoto,[7] Takahiko Murata,[8] Hirokuni Yoshimura,[2] Shuh Narumiya,[8] and Masataka Majima[1]

[1]*Department of Pharmacology,* [2]*Department of Thoracic Surgery,* [3]*Department of Internal Medicine,* [4]*Department of Microbiology, and* [5]*Department of Anatomy, Kitasato University School of Medicine, Kanagawa 228-8555, Japan*
[6]*Minase Research Institute, Ono Pharmaceutical Co. Ltd., Osaka 618-8585, Japan*
[7]*Department of Physiological Chemistry, Faculty of Pharmaceutical Sciences, and* [8]*Department of Pharmacology, Faculty of Medicine, Kyoto University, Kyoto 606-8501, Japan*

Abstract

Nonsteroidal antiinflammatories are known to suppress incidence and progression of malignancies including colorectal cancers. However, the precise mechanism of this action remains unknown. Using prostaglandin (PG) receptor knockout mice, we have evaluated a role of PGs in tumor-associated angiogenesis and tumor growth, and identified PG receptors involved. Sarcoma-180 cells implanted in wild-type (WT) mice formed a tumor with extensive angiogenesis, which was greatly suppressed by specific inhibitors for cyclooxygenase (COX)-2 but not for COX-1. Angiogenesis in sponge implantation model, which can mimic tumor-stromal angiogenesis, was markedly suppressed in mice lacking EP3 ($EP3^{-/-}$) with reduced expression of vascular endothelial growth factor (VEGF) around the sponge implants. Further, implanted tumor growth (sarcoma-180, Lewis lung carcinoma) was markedly suppressed in $EP3^{-/-}$, in which tumor-associated angiogenesis was also reduced. Immunohistochemical analysis revealed that major VEGF-expressing cells in the stroma were CD3/Mac-1 double-negative fibroblasts, and that VEGF-expression in the stroma was markedly reduced in $EP3^{-/-}$, compared with WT. Application of an EP3 receptor antagonist inhibited tumor growth and angiogenesis in WT, but not in $EP3^{-/-}$. These results demonstrate significance of host stromal PGE_2-EP3 receptor signaling in tumor development and angiogenesis. An EP3 receptor antagonist may be a candidate of chemopreventive agents effective for malignant tumors.

Key words: angiogenesis • tumor • prostaglandin E_2 • EP3 receptor • vascular endothelial growth factor

Introduction

Nonsteroidal antiinflammatory drugs (NSAIDs)* that inhibit the enzyme cyclooxygenase (COX) and suppress PG synthesis have been widely used as antiinflammatory, antipyretic, and analgesic agents. Recent epidemiological studies revealed a 40–50% reduction in mortality from colorectal cancer in individuals taking NSAIDs, and evidence suggests that they also affect the incidence and progression of other types of cancer, pointing to a possible role of COX in tumor formation (1). PGs including PGE_2 and PGI_2 comprise a group of oxygenated metabolites of arachidonic acid that are produced by the sequential actions of cyclooxygenase (COX) and specific synthases. Two COX isoforms have been identified: COX-1 is constitutively expressed in various tissues, whereas COX-2 is induced by mitogens, cytokines, and tumor promoters. Disruption of the COX-2 gene in mice reduced the number and size of intestinal polyps generated by a mutation in the adenomatous polyposis (APC) gene, thus verifying a role for COX-2 the generation of colon tumors (2). In spite of the efficacy of NSAIDs as anticancer agents, the precise mechanism(s) for the protective effect remain unknown. An intense debate is underway that focuses on a wide range of mechanisms of antitumor action of

H. Amano and I. Hayashi contributed equally to this work.

Address correspondence to Masataka Majima, Department of Pharmacology, Kitasato University School of Medicine, Kitasato 1-15-1, Sagamihara, Kanagawa 228-8555, Japan. Phone: 81-42-778-8822; Fax: 81-42-778-7604; E-mail: en3m-mjm@asahi-net.or.jp

**Abbreviations used in this paper:* COX, cyclooxygenase; NSAID, nonsteroidal antiinflammatory drugs.

 J. Exp. Med. © The Rockefeller University Press • 0022-1007/2003/01/221/12 $8.00
Volume 197, Number 2, January 20, 2003 221–232
http://www.jem.org/cgi/doi/10.1084/jem.20021408

NSAIDs, some of which are unrelated to inhibition of cyclooxygenase activity (3, 4, 5).

Angiogenesis is an important factor in tumor development, and tumor-associated angiogenesis is mediated by the migration and proliferation of host endothelial cells. With the use of a coculture system comprising endothelial cells and colon carinoma cells that overexpress COX-2, Tsujii et al. (6) showed that the increased production of PGs by the carcinoma cells was associated with endothelial cell migration and tube formation, suggesting a role for COX-2 in tumor-induced angiogenesis. However, the relevance of these in vitro observations to tumorigenesis in vivo remains to be established. Furthermore, whether PGs actually contribute to the observed tumor-associated angiogenesis, and, if so, the identity of the responsible PGs and PG receptors, remains unknown.

For mechanistic analysis of angiogenesis in vivo, we have developed a sponge implantation model, in which a polyurethane sponge disk implanted subcutaneously in rats induces extensive angiogenesis in surrounding proliferative granuloma tissue (7, 8). With the use of this model, we have previously shown that angiogenesis both occurs concomitantly with the induction of COX-2 mRNA and is inhibited by administration either of a nonselective NSAID (indomethacin) or of selective COX-2 inhibitors (9). We further showed that PGE_2 or the PGI_2 analogue beraprost topically injected into the sponge promoted angiogenesis (9). Angiogenesis induced by either endogenous COX-2 or exogenous PGs was accompanied by increased expression of vascular endothelial growth factor (VEGF), and angiogenesis was abolished by administration of an antisense oligonucleotide specific for VEGF mRNA. These results suggest that either PGE_2 or PGI_2 may mediate the angiogenic action of COX-2 in situ.

PGs exert their biological actions by binding to specific receptors that contain seven transmembrane domains. Eight different PG receptors have been defined pharmacologically and cloned, including the PGD receptor (DP), four subtypes of PGE receptor (EP1, EP2, EP3, EP4), the PGF receptor (FP), the PGI receptor (IP), and the thromboxane (TX) receptor (TP) (10). Genes for each of these receptors have been disrupted and the corresponding knockout mice have been produced (11–16). Furthermore, with the use of the cloned receptors, agonists and antagonists highly selective for each of the four EP subtypes have been or are in the process of being developed (17–19).

With the use of these selective compounds and receptor knockout mice, we have now identified the PG species responsible for inducing angiogenesis in the sponge implantation model. Furthermore, we have characterized the role of PG signaling in tumor-associated angiogenesis and tumor progression in a mouse tumor implantation model. Our results indicate that host stromal PGE_2-EP3 signaling appears critical for tumor-associated angiogenesis and tumor growth, and that EP3 signaling pathway is relevant to the induction of a potent proangiogenic growth factor, VEGF, which certainly has a proangiogenic action. A highly selective EP3 antagonist therefore exhibits chemoprevetive action on the stromal cells, and may become a novel therapeutic tool for cancer.

Materials and Methods

Tumor Implantation. Sarcoma 180 cells, which were originally isolated from CFW mice, were cultured at 37°C in RPMI 1640 medium supplemented with 10% fetal bovine serum under a humidified atmosphere containing 5% CO_2. The cells were suspended in phosphate-buffered saline at a density of 5×10^7 cells/ml, and 100 μl of the resulting suspension were injected into the subcutaneous tissue of male mice. Lewis Lung carcinoma cells, which were originally isolated from C57BL/6 mice, were also used in the same manner with sarcoma 180 cells in some experiments (see Fig. 3 F). One half of each specimen was assayed for hemoglobin (Hb) content, whereas the other half was embedded in paraffin, sectioned (5 μm thickness), and stained with factor VIII antibody. Microvessel density was determined following our previous report (20). All animals were housed at a constant temperature (25 ± 1°C) and humidity (60 ± 5%). All experiments were performed in accordance with the guidelines for animal experiments of Kitasato University School of Medicine.

Sponge Implantation Model of Angiogenesis. Sponge disks (thickness, 5 mm; diameter, 1.3 cm; references 7 and 8) were implanted under light ether anesthesia into the subcutaneous tissues of the back of 8-wk-old male ddy mice, male $EP3^{-/-}$ mice (14) and their wild-type counterparts, as well as $IP^{-/-}$ mice (11) and the corresponding WT animals. Neovascularization was assessed by the same method as described above.

Prostaglandin Levels. Fluid within the sponge matrix enclosed by granulation tissue was gently aspirated with the use of a syringe equipped with a 25-gauge needle. The fluid was applied to a Sep-Pak C18 column, and PGs were then eluted with ethyl acetate. The eluate was dried, and the residue containing PGE_2 and 6-keto-$PGF_{1\alpha}$, were assayed with the use of specific ELISA (Cayman Chemical), as reported previously (21).

Immunohistochemistry. Tissue was immediately fixed with 4% paraformaldehyde in 0.1 M sodium phosphate buffer (pH 7.4), dehydrated with a graded series of ethanol solutions, and embedded in paraffin. Sections (4 μm in thickness) were prepared from the paraffin-embedded tissue and mounted on glass slides; after removal of paraffin with xylene, the slides were then placed in cold (4°C) acetone. The sections were subjected to either hematoxylin-eosin staining or immunostaining. For immunostaining, the sections were first exposed to diluted normal horse serum and then incubated with either rabbit antiserum to mouse COX-2 (Cayman Chemical), rabbit antiserum to mouse VEGF (Santa Cruz Biotechnology, Inc.), rabbit antiserum to mouse Mac-1 (BD Biosciences), or rabbit antiserum to mouse CD3e (BD Biosciences). Immune complexes were detected with a Vectastain ABC kit (Vector Laboratories).

In Situ Hybridization. For in situ hybridization, dissected tissue was sectioned with a cryostat, and the resulting sections were fixed with 4% paraformaldehyde. Digoxigenin-labeled antisense and sense riboprobes for mouse EP3 mRNA were prepared by in vitro transcription of the pCRII-TOPO vector (Invitrogen) containing mouse EP3. Sections were treated with proteinase K (10 μg/ml) and were then subjected to hybridization with labeled riboprobes in hybridization solution (Novagen) for 18 h at 50°C in moistened plastic boxes. They were then exposed to RNase A (20 μg/ml) and washed extensively, and hybridized probe was detected by in-